5-1-2015

HOLOCENE FORAMINIFERAL ASSEMBLAGE AND STABLE ISOTOPE ANALYSIS FOR THE GERLACHE STRAIT, ANTARCTIC PENINSULA

Daniel James Groves
Southern Illinois University Carbondale, djgrove@siu.edu

HOLOCENE FORAMINIFERAL ASSEMBLAGE AND STABLE ISOTOPE ANALYSIS FOR THE GERLACHE STRAIT, ANTARCTIC PENINISULA

by

Daniel J. Groves

B.S., Illinois State University, 2013

A Thesis
Submitted in Partial Fulfillment of the Requirements for the
Masters of Science Degree

Department of Geology
in the Graduate School
Southern Illinois University Carbondale
May 2015

THESIS APPROVAL

HOLOCENE FORAMINIFERAL ASSEMBLAGE AND STABLE ISOTOPE ANALYSIS FOR THE GERLACHE STRAIT, ANTARCTIC PENINISULA

By

Daniel J. Groves

A Thesis Submitted in Partial

Fulfillment of the Requirements

for the Degree of

Masters of Science

in the field of Geology

Approved by:

Dr. Scott Ishman, Chair

Dr. Liliana Lefticariu

Dr. Nicholas Pinter

Graduate School
Southern Illinois University Carbondale
April 10, 2015

AN ABSTRACT OF THE THESIS OF

Daniel J. Groves, for the Masters of Science degree in Geology, presented on April 10, 2015, at Southern Illinois University Carbondale.

TITLE: HOLOCENE FORAMINIFERAL ASSEMBLAGE AND STABLE ISOTOPE ANALYSIS FOR THE GERLACHE STRAIT, ANTARCTIC PENINSULA

MAJOR PROFESSOR: Dr. Scott Ishman

The Antarctic Peninsula is one of the fastest warming regions on the planet. In the past 50 years, the temperature has increased by more than 2^{o} C, leading to the retreat of large areas of the ice shelves fringing the Antarctic Peninsula. Recent environmental changes in the Antarctic Peninsula are well documented by meteorological and remote sensing data, but the behavior of the Holocene atmosphere-ocean-cryosphere system is not well understood. In this study, foraminifera are used as a proxy for Holocene oceanographic conditions in the Gerlache Strait, western Antarctic Peninsula. The most abundant foraminifera identified in this study include the agglutinated taxa *Miliammina arenacea* and *Paratrochammina lepida,* which are associated with cold, saline water masses and periods of high sea-ice production. The most abundant calcareous species identified is the opportunistic *Fursenkoina* spp., which is associated with ice-proximal conditions and freshwater input due to glacial melting.

This study shows deglaciation of the Gerlache following the Last Glacial Maximum at ~7700 ± 20 cal. years BP, indicated by the appearance of foraminifera and diatoms. The post-deglaciation period is characterized by high-frequency variation in foraminiferal assemblages between abundant agglutinated and calcareous taxa, indicating unstable glacial conditions. The beginning of the Mid-Holocene Climatic Optimum (MHCO) is indicated by a substantial

decrease in sedimentation rates and a shift to more stable foraminiferal assemblages. A decline in diatom abundance and the absence of calcareous foraminifera indicate a glacial readvance at 6030 ± 20 cal. years BP. At 4470 ± 20 cal. years BP the calcareous taxa including *Fursenkoina* spp. become dominant, indicating glacial retreat and input of fresh water into the water column. After 3240 ± 15 cal. years BP agglutinated taxa are once again dominant and calcareous taxa absent. This marks the beginning of the Neoglacial period and the presence of colder, more saline shelf waters in the Gerlache Strait. Stratification of the water column is apparent during the Post-Deglaciation period and the latter part of the MCHO. A difference in $\delta^{18}O$ values of >0.5 ‰ between benthic and planktonic foraminifera indicates the presence of an isotopically lighter surface water layer which may be the result of freshwater input due to glacial melting and an estuarine circulation regime.

TABLE OF CONTENTS

LIST OF TABLES

TABLE PAGE

LIST OF FIGURES

FIGURE PAGE

CHAPTER 1

INTRODUCTION

The Antarctic Peninsula (AP) has a dynamic climate. The small size and lower latitude of the AP results in cryospheric and ecological systems that are more sensitive to climatic changes relative to the rest of Antarctic mainland (Smith et al., 1999; Domack et al., 2001; Ingolfsson et al., 2003). Recent warming (>2^{o} C) over the past 50 years has led to acceleration in ice-shelf retreat (Stark, 1994; Ingolfsson, 2003). Rapid disintegration of 3320 km^2 from the Larsen B Ice Shelf in 2002 illustrates the rate and scale at which ice shelf-breakups can occur (Scambos et al., 2003). Current environmental changes in the AP are documented by meteorological and remote-sensing data, but the behavior of the Holocene-scale atmosphere-ocean-cryosphere system is not well understood (Domack et al., 2003).

During the Last Glacial Maximum (LGM), ice sheets were grounded along the AP continental shelf. The timing of deglaciation of the AP following the LGM is not well constrained, and estimates range from 11 to 4.5 cal. ka (Pudsey et al., 1994; Hjort et al., 1997). The variability of climate during the Holocene is complex and involves warming and cooling at different rates and times across the AP (Davies et al., 2012). The western AP continental margin provides an opportunity to study the Antarctic Holocene paleoclimate (Leventer et al., 1996; Domack et al., 1998; Ishman and Sperling, 2002). Pleistocene glaciation of the AP led to the formation of fjords and deep inner-shelf basins or troughs (Rebesco et al., 1998; Anderson, 1999; Barker et al., 1999; Domack et al., 2003). Glaciomarine sediment accumulated in these basins, leaving a record of environmental conditions during the Holocene (Ishman and Domack, 1994).

This study will focus on the sediment core LMG 12-11 JPC-3 from the Gerlache Strait, off of the western coast of the AP (Figure 1.1). Analysis of foraminiferal assemblages and stable-oxygen isotope data provides a high-resolution chronology of Holocene paleoenvironmental conditions. Obtaining a high-resolution chronology of glacial events and paleoceanographic conditions is significant as part of a larger study to determine if recent ice-shelf collapse is unique or if similar events have occurred in the past. Understanding the behavior of the glacial system in the past is essential for our understanding of the processes that control glacial fluctuations today (Ingolfsson et al., 2003). In order to go from modern observations to a predictive model, we must understand the behavior of the climate-ocean-ice system in a paleoenvironmental context (Domack et al., 2003). This research is part of an interdisciplinary study, LARISSA (LARsen Ice Shelf System, Antarctica), which aims to understand the processes of the climate-ocean-ice system in the AP that respond to and affect modern environmental change.

Setting:

The AP stretches 1250 km north from Antarctica towards the southern tip of South America, from 75° S to 62° S (Fig. 1.1). Its maximum width is less than 250 km, ranging from 55° W to 80° W, and including the South Shetland Islands and the Northwestern Weddell Sea (Figure 1.2; Domack et al., 2003; Ingolfsson et al., 2003). The Gerlache Strait is up to 40 km wide and 120 km long and is 300 m deep in the southwest, deepening to 1200 m deep in the northeast (Evans et al., 2004). The strait runs between the Danco Coast area of the northwest

AP and Anvers and Brabant Islands, which separate the strait from the Palmer Archipelago (Evans et al., 2004). The Gerlache Strait is a western continuation of the southwest-northeast Bransfield Basin (Canals, 2000). The Bransfield Basin (Figure 1.2) extends from 61°58'S, 56°18W to 64°47'S, 63°32'W and is approximately 100 km wide and 450 km long (Banfield and Anderson, 1995). Modern extension in the Bransfield Basin is the result of the sinistral movement between the Scotia and Antarctic plates (Gonzalez-Cosado et al., 2008).

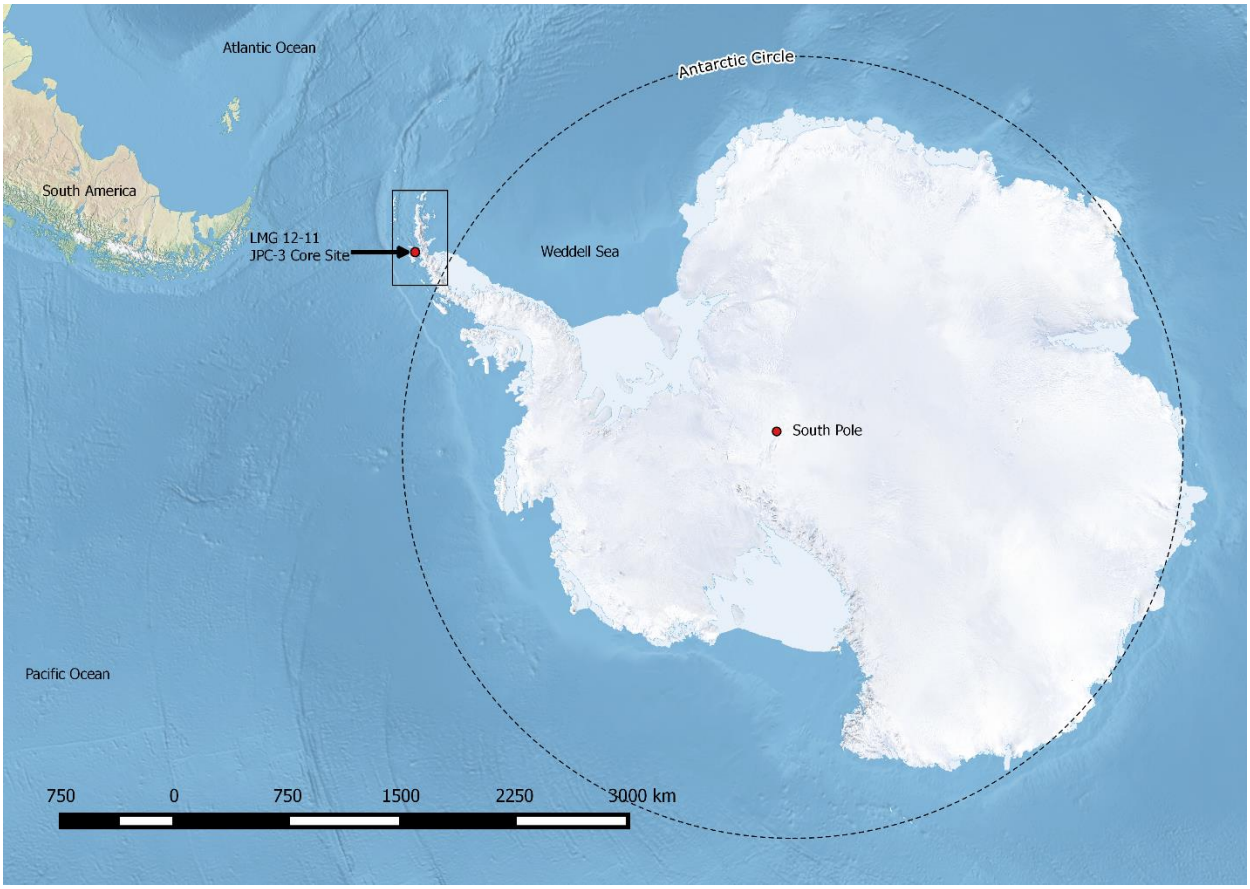

Figure 1.1: Map of Antarctica with the study region and LMG 12-11 JPC-3 Core Site

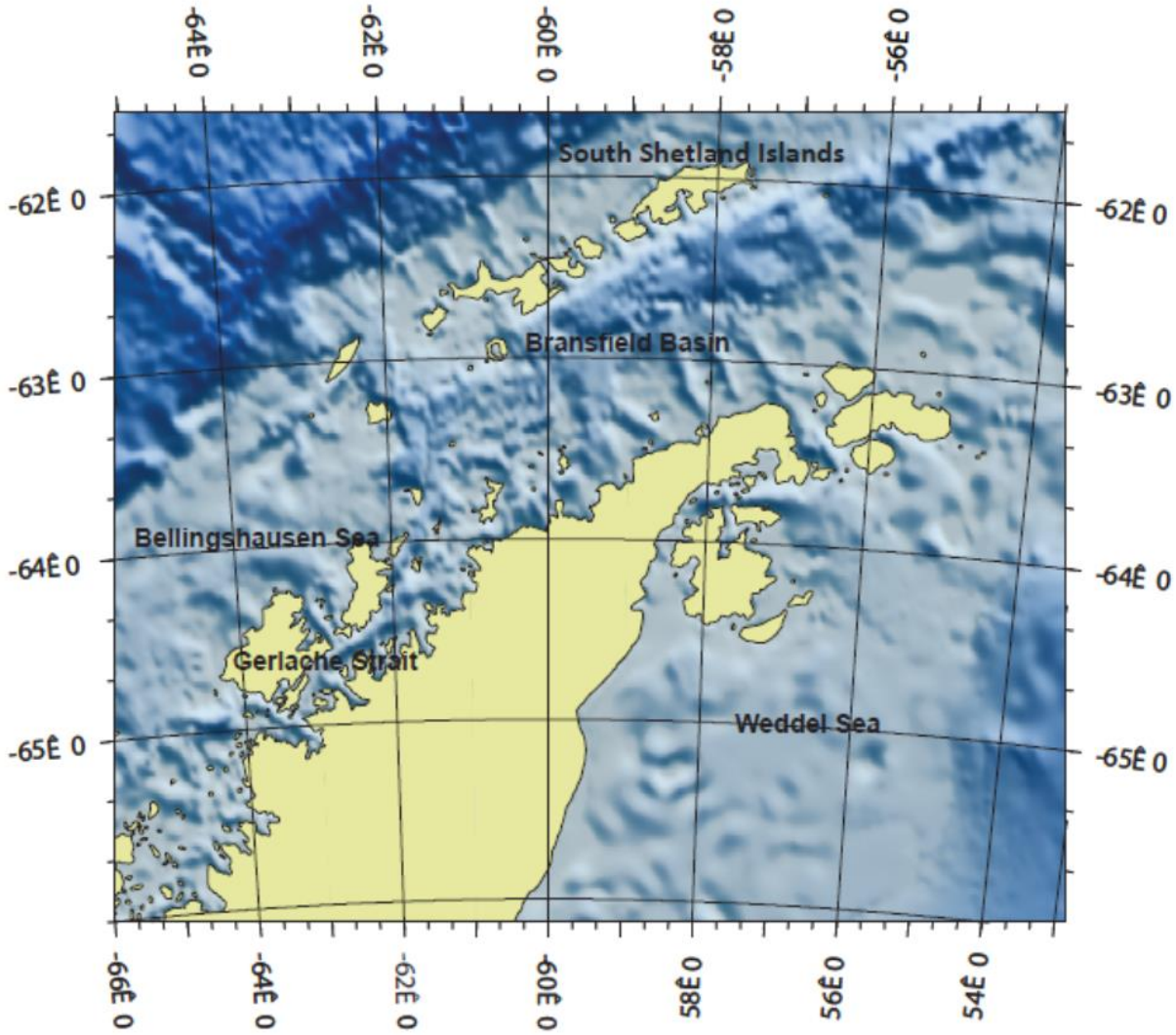

Figure 1.2: Map of the Northern portion of the AP with bathymetry of the shelf.

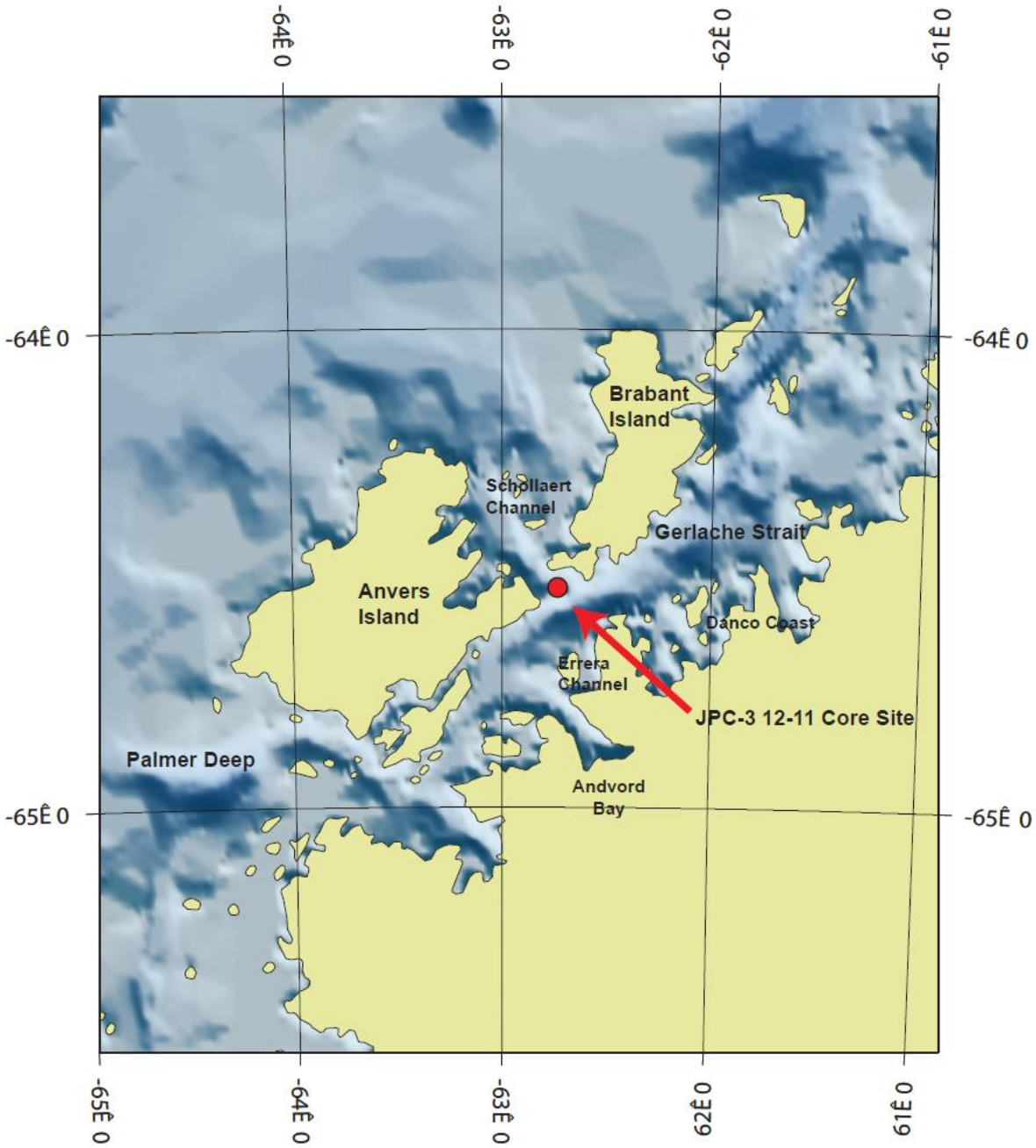

Figure 1.3: Map of the study area with bathymetry of the shelf. The JPC-3 12-11 Core Site in red.

Geology:

The basement rock of the AP consists of intermediate-grade metamorphic rocks formed in an accretionary prism during the Mesozoic. (Domack et al., 2003). During the late Paleogene, a reorganization of seafloor spreading led to uplift and dissection of Mesozoic igneous and metamorphic rocks (Elliot, 1997; Domack et al., 2003). This uplift may have encouraged the development of ice sheets across the AP. The late Paleogene change in seafloor spreading also led to the separation of the Andes and the AP, and the creation of the Drake Passage (Eagles and Livermore, 2002; Davies et al., 2012). The opening of the Drake Passage allowed for the formation of the Antarctic Circumpolar Current, which may have contributed to the development of Antarctic ice sheets (Kennett et al., 1975; Siegert, 2008; Davies et al., 2012). Pleistocene glaciation of the AP led to the formation of fjords and deep inner shelf basins or troughs (Rebesco et al., 1998; Anderson, 1999; Barker et al., 1999; Domack et al., 2003) where glaciomarine sediment accumulated during the Holocene (Ishman and Domack, 1994).

Accumulations of pelagic, hemipelagic, and ice-rafted sediment cover the continental shelf of the Gerlache Strait (Wilmott et al., 2007). The two mapped sediment drifts in the Gerlache Strait are the Andvord and the Schollaert Drifts. The Andvord Drift, adjacent to Andvord Bay (Figure 1.3), covers an area of 45 km^2 to a maximum thickness of 40 m. Modern sedimentation rates of 1-3 mm/yr suggest that the total thickness of the deposit is postglacial. (Harris et al., 1999). The drift is 17 km long and ranges from 0.5 to 5 km wide (Harris et al., 1999). The Andvord Drift consists of 3 lobes: extending into the Andvord Bay, the Gerlache Strait, and toward the Errera Channel. Sedimentation rates based on ^{14}C profiles have been calculated at 3 core sites located within the Andvord Bay lobe. Through the late Holocene these

rates range from 1.5 to 3.2 mm/yr (Harris et al., 1999). More recent sedimentation rates, from the top of cores, based on ^{210}Pb profiles range from 1.5 to 1.8 mm/yr (Domack and Mammone, 1993). The Schollaert Drift is located between Anvers Island and the Danco Coast (Fig. 1.3); its maximum thickness is 70 m, and it is 6 km in length (Canals et al., 1998; Wilmott et al., 2007). Sediment cores from the Schollaert and Andvord Drifts show two major sedimentary units. Unit I consists primarily of massive bioturbated diatom mud and ooze. Unit II underlies Unit I and is characterized by alternating laminations of sandy mud and diatom ooze (Wilmott et al., 2007). Preservation of these laminations is thought to be a result of higher sedimentation rates and stratification of the water column due to estuarine conditions during the middle Holocene (Yoon and Chough, 1993; Laberg and Vorren, 2004; Wilmott et al., 2007).

Climate and Cryosphere:

The AP today is 80% covered by ice (Bindschadler, 2006; Davies et al., 2012). The ice sheet is ~500 m thick, with outlet glaciers on its east and west sides (Davies et al., 2012). More than 80% of the AP ice sheets drain to the surrounding ice shelves. Ice shelves can be affected by changes in atmospheric conditions at the surface, or by exposure to warm water at depth. Exposure to warm water can result in loss of mass due to basal melting (Pritchard et al., 2012).

The mountains of the AP, with an average height of 1500 m, form a barrier to moist westerly winds. This barrier creates a gradient of climate conditions across the Peninsula, from a polar-maritime climate on the west to a polar-continental climate on the east (Reynolds, 1981; Morris and Vaughan, 2003; Vaughan et al., 2003; Summerhayes et al., 2009; Davies et al.,

2012). The western side of the Peninsula experiences more snow accumulation and higher summer temperatures. The eastern side experiences less snowfall and lower summer temperatures. Because the eastern AP receives less snowfall, the ice shelves are more vulnerable to short-term changes in climate (Domack et al., 2003).

Oceanography:

The eastern and western sides of the AP also differ in their oceanographic characteristics. The western side of the AP contacts a comparatively warm (>1.5^{o} C) and deep body of water known as the Circumpolar Deep Water (CDW). The Upper Circumpolar Deep Water (UCDW) comes from upwelling associated with the impingement of the Antarctic Circumpolar Current (ACC) onto the western AP continental shelf and mixing of CDW with shelf waters. The proximity of the ACC to the western AP continental shelf, along with the west-to-east flow of the ACC, creates a pressure gradient that pushes water onto the shelf through submarine canyons (Hofmann and Klinck, 1998). The ACC is known to shift locations in the Drake Passage yearly and also at longer time scales (Hofmann and Whitworth, 1985; Klinck and Smith, 1993). This fluctuation affects the extent to which the UCDW impinges onto the shelf (Hofmann and Klinck, 1998). Incursion of the UCDW has been shown to cause basal melting and ice shelf disintegration (Pritchard et. al. 2012).

The southernmost region of the ACC contacts another bottom-water mass known as the Weddell Sea Transitional Water (WSTS), which is colder (<-1.0^{o} C) and more saline than the UCDW. This boundary ranges from the southern Bransfield Strait to the southern Gerlache

Strait (Hoffman and Klinck, 1998; cited by Domack et al., 2003). There is also a distinction between the UCDW and a cooler water mass with temperatures of less than 0^{o} C and salinities of 34.45-34.6 ppt. This water mass is referred to as Bransfield Strait water. It is found in the Bransfield Strait and is derived from waters originating in the Weddell Sea (Whitworth et al., 1994; Hoffman and Klinck, 1996).

UCDW is present along much of the western AP continental shelf. Waters characteristic of the UCDW enter the western Bransfield Strait through the passageway between the South Shetland Islands and also extend along the southern portion of the South Shetland Islands. The penetration of UCDW is limited into the main portion of the Bransfield Strait (Hoffman and Klinck, 1996). There is a strong temperature boundary between the UCDW and the colder Bransfield Strait water in the Bransfield Strait (Capella et al., 1992, Stein and Heywood, 1994).

Individual surface water masses on the western AP continental shelf are defined by their thermohaline characteristics. The Antarctic Surface Water (AASW) is defined by a minimum temperature of -1.5 to -1.8^{o} C and salinities ranging from 33.9 to 34.0 ppt. (Gordon et al., 1977). The surface waters on the western AP continental shelf are seasonally variable. Thermohaline changes in water shallower than 150 m occur due to exchange with the atmosphere, changes in solar heating and the formation and melting of sea ice (Hoffman and Klinck, 1998). During the winter AASW remains near -1.8^{o} C. In the summer and fall, solar warming of the surface waters isolates AASW to a depth of 100 m, shallowing shoreward. This isolated layer of AASW is known as the Winter Water (WW) and has a minimum temperature below 0.0^{o} C (WW; Mosby, 1934;

Sievers and Nowlin, 1984). The water masses deeper than 150 m are the UCDW and a modified, cooler UCDW formed from mixing with WW (Hoffman and Klinck, 1998).

Two water masses with different salinities occur on the shelf of the Weddell Sea on the eastern side of the AP. One is the Hyper Saline Shelf Water (HSSW), which has a salinity of ~34.7 ppt and a temperature of ~1.9^{o} C and is a result of sea-ice production. The lower salinity (34.6 ppt) water mass, known as the Ice Shelf Water (ISW), is a product of sea ice melting and ranges in temperature from 1.4-1.8^{o} C (Gordon, 1998; Scymcek, 2007). These water masses were first described on the eastern AP continental margin, but they have been identified in the paleorecord of the western AP in the Palmer Deep (Ishman and Sperling, 2002). Because the ISW and HSSW are products of glacial advance or retreat, they can be very useful in determining past glacial conditions.

The Last Glacial Maximum (LGM) deglaciation and Holocene paleoclimate:

During the last glaciation of the Gerlache Strait, the AP ice sheet was drained by paleo-ice streams that grounded across the continental shelf (Pudsey et al., 1994; Bentley and Anderson, 1999; Canals et al., 2000, 2002; O´ Cofaigh et al., 2002; Dowdeswell et al., 2004; Evans et al., in press; Evans et al., 2004). Existence of a major paleo-ice stream in the Bransfield Basin, just north of the Gerlache Strait, is evident in mega-scale glacial landforms called bundle structures. These structures form by accumulation of basal deformation till below an ice stream (Canals, 2000). Seismic facies analysis in the Bransfield Basin shows that ice was grounded on the shallow inner shelf (Banfield and Anderson, 1995). Streamlined bedforms in the Gerlache

Strait, including drumlins and other crudely streamlined forms, were formed when the ice sheet last filled the strait. Ice drained from the AP ice sheet through tributary bays along the Danco Coast and into the Gerlache Strait. The streamlined bedforms have a northeast-southwest orientation, indicating a northeasterly direction of ice flow through the strait (Evans et al., 2004).

The beginning of the Holocene is marked by increased temperatures along the AP continental shelf. Stable isotope records from ice cores in Antarctica show an early Holocene climatic optimum between 11 and 9.5 cal. ka (Ciais et al., 1992; Masson et al., 2000; Masson-Delmotte et al., 2004; Bentley et al., 2009). The timing of the onset of deglaciation on the AP continental shelf is constrained to minimum ages based on the oldest ^{14}C dates. Organic carbon of diatomaceous mud from the Bransfield Basin gave ^{14}C dates indicating ice retreat prior to 13-14 cal. ka (Banfield and Anderson, 1995). Palmer Deep records based on ^{14}C of foraminiferal calcite showed that inner shelf areas may have deglaciated by 11 cal. ka (Domack et al., 2001). Dates for deglaciation of the innershelf fjords and bays are as late as 6-8 cal. ka (Harden et al., 1992; Pudsey et al., 1994; Shevenell et al., 1996; Hjort et al., 2001; Ingolfsson et al., 2003). Glacial-marine sedimentation began in the Gerlache Strait after 8 cal. ka, based on ^{14}C dates of diatomaceous sediment (Harden et al., 1992). In Lallemand Fjord, south of the Gerlache, glaciomarine sedimentation began around 8 cal. ka according to ^{14}C dating of a scaphopod shell (Shevenell et al., 1996). Benthic foraminiferal assemblages appear in the Palmer Deep 12.6 ka, whereas diatoms appear earlier at 13.2 ka. These findings indicate retreat of the LGM ice shelf from the Palmer deep at 13.2 ka and benthic activity beginning at 12.6 ka (Ishman and Sperling, 2002). While much of Antarctica was experiencing a warm period in the early Holocene, the

Palmer Deep record from this time shows a period of colder water. Diatom and foraminiferal assemblages show that cold shelf water occupied the Palmer deep through the early Holocene (Ishman and Sperling, 2002; Sjunneskog and Taylor, 2002; Taylor and Sjunneskog, 2002).

Following the initial climatic optimum, the climate was variable across the AP. Deglaciation was ongoing during this period, but at a slower rate, leading up to the Mid-Holocene Climatic Optimum (MHCO), from 4.5 to 2.8 cal. ka (Bentley et al., 2009). The MHCO has been identified in Lallemand Fjord as a period of higher primary productivity, marked by higher percent Total Organic Carbon (% TOC) in marine sediments (Shevenell et al., 1996). Domack et al. (2003) identified elevated % TOC in Lallemand Fjord associated with this warm period before 2.5 cal. ka, likely caused by increased primary productivity due to changes in sea-ice extent. Records from the Prince Gustav Channel ice channel from 2 to 5 cal. ka indicate that the ice shelves had retreated, allowing for movement of icebergs and the deposition of ice-rafted debris. There is also evidence for the destabilization of the Larsen-A ice shelf between 4000 and 1400 cal. years BP (Pudsey and Evans, 2001; Brachfeld et al., 2003; Pudsey et al., 2006). The record from the Palmer Deep shows a much longer warm period, indicated by higher primary productivity and a decrease in ice-rafted debris, ranging from 9 to 3.6 ka. This may represent the continuous presence of the relatively warm Upper Circumpolar Deep Water (UCDW) on the continental shelf during this time (Domack et al., 2002). Ishman and Sperling (2002) argue that benthic foraminiferal assemblages from the Palmer Deep indicate cold saline shelf water in the absence of UCDW, while diatom data indicate a seasonal surface-water with high primary productivity.

A Neoglacial period has been proposed between 2.5 and 1.3 cal. ka (Bentley et al., 2009). Glaciers readvanced into Lallemand Fjord at 2.5 cal. ka, productivity decreased after 3 cal. ka, and diatom abundances suggest an increase in sea ice after 2.7 cal. ka (Domack and McClennen, 1996; Shevenell et al., 1996). The Prince Gustav Channel and Larsen-A ice shelves also began to reform at 1900 and 1400 cal. years BP, respectively (Pudsey and Evans, 2001; Brachfeld et al., 2003; Pudsey et al., 2006). The Palmer Deep record shows an earlier beginning to the Neoglacial period, indicated by an increase in mass-accumulation rate and coarse-fraction ice-rafted debris (Domack, 2002). In the Bransfield Strait, an increase in sea-ice taxa of siliceous microfossils has been associated with cooler temperatures (Barcena et al., 1998). Christ et al. (2014) constrain the beginning of the neoglacial in Barilari Bay, south of the Gelrache, to 2815 cal. years BP based on a decrease in diatom abndance and an increase in ice-rafted debris.

The Medieval Warm Period (MWP) has been identified in the Northern hemisphere from 1.2 to 0.6 cal. ka but is not strongly expressed in Antarctic records (Bentley et al., 2009). The marine record from Lallemand Fjord shows a smaller % total organic carbon (%TOC) maximum following the maximum associated with the MHCO. This is interpreted to have been caused by higher productivity during the MWP (Domack et al., 2003). A core from the Bransfield Basin had increased magnetic susceptibility during 700 to 970 cal. years BP, indicating warmer temperatures (Khim et al., 2002). The Palmer Deep record also indicates a “Little Ice Age” from 700 to 150, cal. years BP with evidence for more persistent sea ice and colder bottom and surface water conditions (Shevenell et al., 1996; Shevenell and Kennett, 2002; Domack et al., 2003). The Little Ice Age was also identified in Barilari Bay beginning 730 cal. years BP and is

characterized by a shift to ice-proximal turbidite deposits and decreased primary productivity (Christ et al., 2014).

Foraminifera as Environmental Indicators:

Antarctic benthic foraminiferal distributions have been shown to be controlled by water-mass characteristics (Ishman and Domack, 1994; Szymcek et al., 2007; Ishman and Sperling, 2002). Modern benthic foraminiferal assemblages on the AP western margin have been associated with two dominant water masses, the UCDW and WSTW. This association makes it possible to discern water-mass characteristics in the Holocene based on foraminiferal assemblages (Ishman and Domack, 1994). Glacier-produced HSSW and ISW have been associated with modern foraminiferal assemblages on the eastern shelf, and similar water masses can be interpreted in the paleorecord on the western AP shelf (Milam and Anderson, 1985; Ishman and Sperling, 2002: Ishman and Szymcek, 2003; Szymcek et al., 2007).

Water-mass characteristics are often a result of sea-ice and glacial conditions, making foraminiferal assemblages useful as indicators of ice-shelf extent. Assemblages dominated by agglutinated taxa, including the *Miliammina arenacea* assemblage described by Ishman and Sperling (2002), have been associated with cold, corrosive bottom water, such as the HSSW, which is indicative of high sea-ice production (Anderson, 1975). Assemblages dominated by opportunistic taxa, including the *Fursenkoina fusifomis* assemblage described by Ishman and Sperling (2002), may be indicative of increased organic flux to the substrate associated with near-ice conditions and ice-shelf retreat. The *Stainforthia fusiformis* assemblage, described by

Szymcek et al. (2007), is dominated by calcareous taxa, indicating the production of the less saline ISW associated with the melting of glacial ice.

In addition to assemblage analysis, stable-oxygen isotope analysis of foraminiferal calcite can provide information about paleoenvironments. The temperature of the water in which calcium carbonate precipitates has an effect on $\delta^{18}O$ values (Berger, 1979). The difference in $\delta^{18}O$ values between calcite and seawater decrease with increasing temperature (Berger, 1979). This allows for the calculation of paleotemperature based on $\delta^{18}O$ values of foraminiferal calcite. Because consistent temperatures near 0^{o} C can be assumed during the Holocene (Domack, 2005), changes in $\delta^{18}O$ values can be attributed to the variability of water column salinity associated with ice-volume conditions. Depletion of $\delta^{18}O$ in foraminifera is indicative of a reduction in salinity of the water column due to melting and thinning of the ice shelf (Domack et al., 2005). We hypothesize that foraminiferal assemblage and isotope data will reflect temporal change in paleoenvironmental conditions, including temperature and salinity of water masses, and primary productivity. These changes in paleoenvironment may be associated with a reduction in ice-shelf extent due to incursion of the UCDW onto the AP continental shelf during the Holocene.

CHAPTER 2

MATERIALS AND METHODS

Jumbo Piston Core 3 (JPC-3) was collected from the RV *Laurence M. Gould* during the LMG 12-11 cruise in the fall of 2012. The core was analyzed for diatom assemblages by Bianchini (unpublished, 2014) and Leventer (unpublished, 2015). Radiocarbon analysis was conducted on core JPC-3 by Domack (unpublished, 2015), using mollusk shells from 4 depths in the core. The core site is in the Gerlache Strait, off of the west coast of the AP, at latitude 64^{o} 39.660' S and longitude 62^{o} 54.760' W (Fig. 1.3). The core was collected from a water depth of 710 m, with 1025 cm of sediment recovered. The core consists mostly of an olive grey laminated diatom mud and ooze, with some pebbles. The bottom 1 m of the core contains coarse sand, fining upward to silt and mud (Figure 2.1).

A 1.0 cm-thick sample was collected every 10 cm for foraminiferal analysis. A total of 91 samples were washed through a 63 μm sieve, leaving foraminifera of size 63 μm or greater. The 63 μm fraction has been shown to include smaller species of foraminifera (Schroder at al., 1987). Planktonic and benthic foraminifera were collected from each sample and identified based on the taxonomic concepts of Igarashi et al. (2001) and Majewski (2005). A total of 300 foraminifera were collected from each sample, unless the sample did not contain 300 specimens. In samples containing fewer than 300 individuals, as many were collected as possible. A sample size of 300 specimens has been shown to be statistically sufficient to represent species, which comprise ≥ 1% of the total sample (Dennison and Hay, 1967). Total foraminiferal counts for each sample can be found in Appendix B.

Figure 2.1a: Images of core JPC-3 form the top of the core to 455 cm.

Figure 2.1b: Images of core JPC-3 from 455 cm to the base of the core.

Isotope Analysis:

Stable-oxygen isotopic values were determined for samples with sufficient biogenic calcium carbonate to yield a result. Dr. Michael Prentice conducted isotope analysis. Measurements were taken using the Finnegan MAT 252 gas-mass spectrometer fitted with a Kiel III carbonate preparation system in the Benedum Stable Isotope Laboratory of Brown University following standard procedures. The stable isotope ratios of oxygen are expressed in routine $\delta^{18}O$ notation in per mil (‰) relative to VPDB (Coplen, 1996):

$$\delta^{18}O = [(R\ sample - R\ standard) * 1000]/R\ standard$$

R sample and R standard refer to the $^{18}O/^{16}O$ ratios in the samples and standard, respectively.

Analytical precision was determined to be 0.08 ‰ based on replicate analyses of the NBS-19 and BYM standards. The planktonic *N. pachyderma* and the benthic *Globocassiduina* spp. were used for isotopic analysis. The two species were analyzed separately in groups of two to ten. Uncertainty (2σ) for individual taxa based on replicate analyses is ± 0.1 ‰.

CHAPTER 3

RESULTS

Sedimentology:

The bottom of the core, from 987 to 975 cm, is composed of olive-grey laminated mud and fine sand with no fossil content. Pea-sized gravel at 975 cm grades upwards to fine sand at 913 cm. From 913 to 903 cm, the core contains laminated rythmites of very fine sand and silt, overlain by streaky mud until 890 cm. At 890 cm there is an abrupt transition to very coarse sand, which fines upward to olive-grey mud at 881 cm. The mud is a diatom mud or ooze, and is mostly homogeneous until 756 cm, above which laminated muds occur until 731 cm. From 731 cm to 605 cm, laminated muds are interstratified with unlaminated muds. Between 605 cm and 210 cm, the mud is laminated, with some shorter homogeneous intervals. Above 210 cm the diatom mud is unlaminated, with bioturbation until 126 cm. The interval from 126 cm to the top of the core is homogeneous, with some large pebbles. Coarse sand and gravel occur occasionally throughout the core as dropstones.

Foraminifera:

This study identified 39 species and open-nomenclature taxa of foraminifera, including 17 calcareous benthic, 21 agglutinated benthic, and 1 calcareous planktonic foraminifer. Of the 92 samples, 34 yielded at least 300 specimens. The smallest number of specimens collected from a sample was 6 and the average was 208. Species abundance is low, with as few as two

species in a sample. Species diversity peaks at 540 cm, with 25 species, and levels off in the top 2 m, to between 11 and 16 species. Agglutinated taxa are abundant, accounting for 72 % of the specimens collected. Common agglutinated species include: *M. arenacea*, *Portatrochammina lepida*, *Paratrochammina antarctica,* and *Spiroplectammina biformis*. Calcareous taxa are less abundant, but still account for 28 % of the specimens collected. Common calcareous species include *Fursenkoina* spp., *Globocassidulina* spp., *N. pachyderma*, and *Nonionella iridea*. In this study, *Fursenkoina* spp. includes *F. fusiformis* and, much less frequently occurring *F. vestfoldensis*. *Globocassidulina spp*. includes the two similar species *G. subglobosa* and *G. biora*. The most common taxa overall were *M. arenacea* (29.85 % of total specimens), *Paratrochammina lepida* (23.66 %), *Fursenkoina* spp. (14.14 %), *Globocassidulina* spp. (4.88 %), and *N. iridea* (3.04 %).

M. arenacea was present in every sample, comprising 100% of the specimens in some samples (Figure 3.1). *P. lepida* is nearly non-existent in the basal samples, but increases in abundance beginning at 280 cm and remains abundant shallower in the core, averaging 35 % from 280 cm to the top of the core. *P. lepida* reaches abundances of >60 % at 90 cm, 260 cm, and 390 cm. The presence of *Fursenkoina spp*. in the core is sporadic, with intervals of total absence interrupted by intervals where abundance reaches as high as 61 %. Peaks in *Fursenkoina* spp. abundance coincide with peaks in other calcareous taxa including *Globocassidulina* spp., *N. iridea,* and *N. pachyderma.*

The base of the core is dominated by calcareous foraminifera (Figure 3.2). From 841 to 290 cm longer intervals of mostly agglutinated foraminifera are interrupted by shorter,

calcareous-dominated intervals. Few calcareous forms occur above 281 cm. Total foraminifer abundance was variable but appears to decrease with depth.

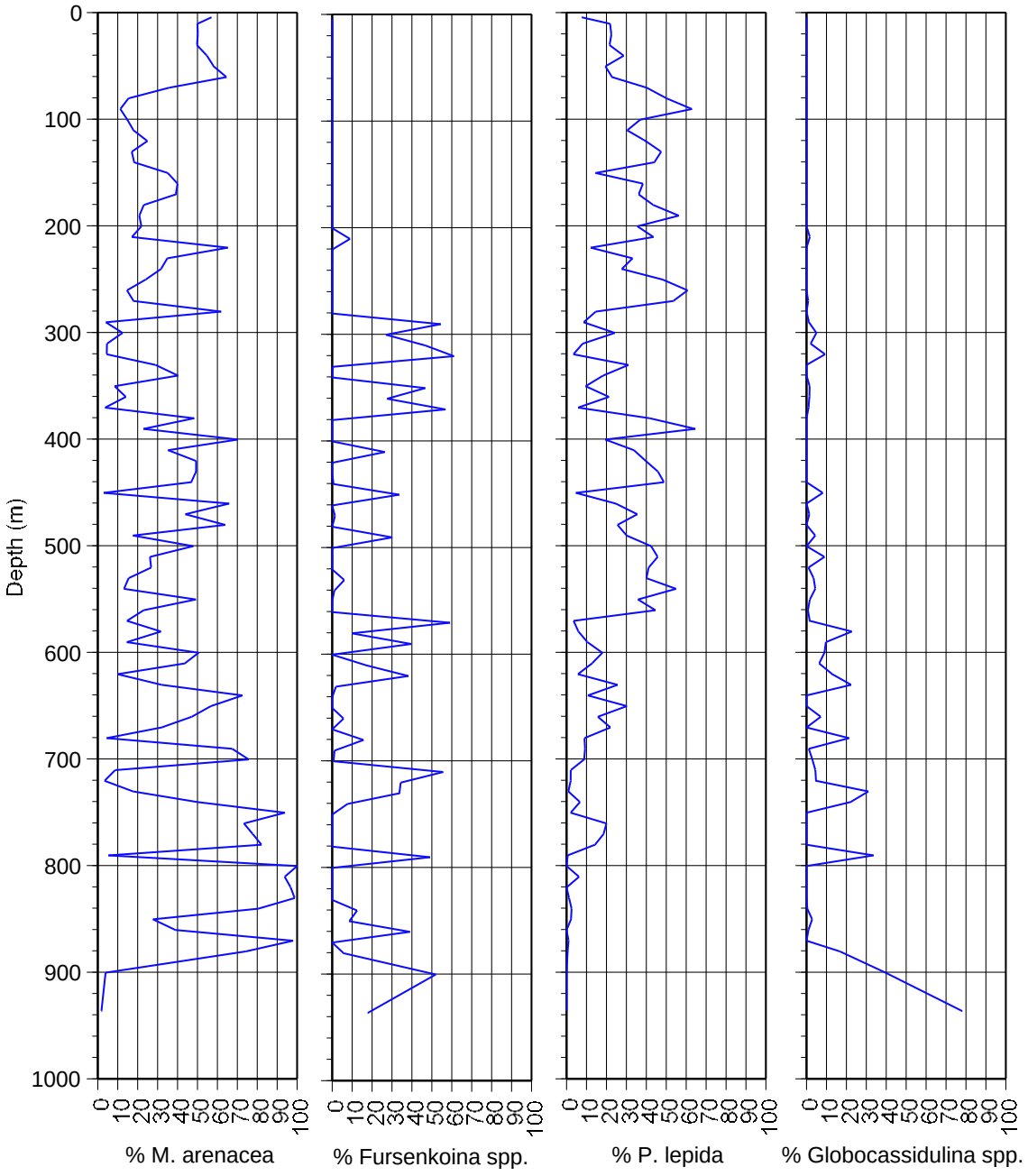

Figure 3.1: Percent abundances of the 4 most common species.

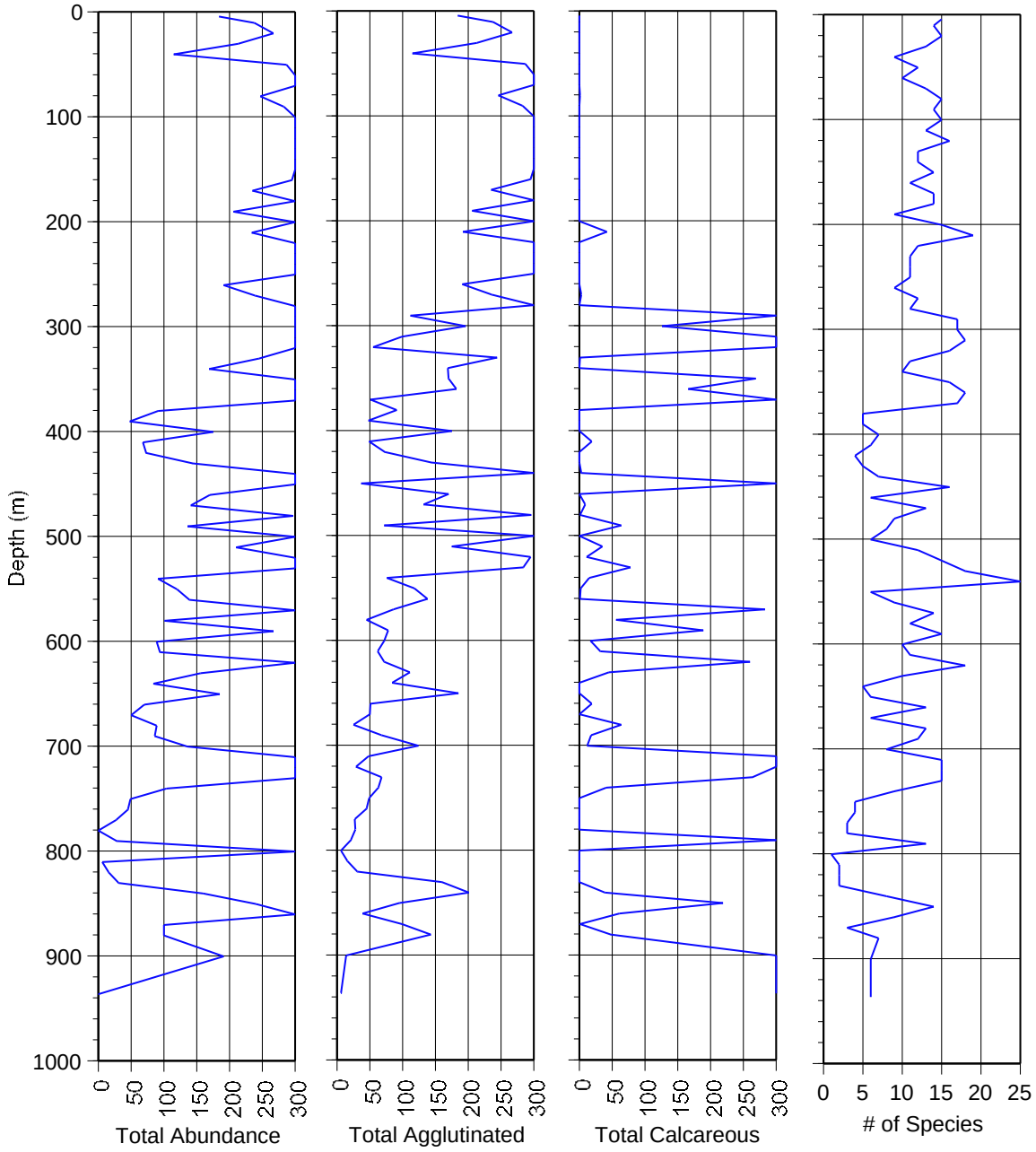

Figure 3.2: Total abundance, abundance of agglutinated specimens, abundance of calcareous specimens, and the total number of species in each sample.

Age model:

The age model used in this study is based on radiocarbon dates obtained from mollusk shell fragments at 4 depths (Table 3.1). Ages are calibrated by the method outlined in Stuiver and Polach (1977), using unreported ^{13}C values. The calibrated ages are also reservoir corrected by 350 years based on the ^{14}C age of a modern mollusk shell collected from Oneida Lake (Leventer, personal communication, 2015). Below 481 cm, sedimentation rates are calculated to be 0.37 cm/yr. Between 481 cm and 345 cm, sedimentation rates decrease by nearly an order of magnitude, to 0.05 cm/year. Above 345 cm rates increase slightly to 0.09 cm/yr. These sedimentation rates compare favorably to rates in the nearby Andvord Drift of 0.1 to 0.3 cm/yr (Harris et al., 1999). Modern sedimentation rates based on ^{210}Pb profiles were determined to be 0.15 to 0.18 mm/yr, also in Andvord Bay (Domack and Mammone, 1993). The time model assigned to the core is based on the calculated sedimentation rates, and ages are cited in calibrated years before present (cal. years BP; Figure 3.3).

Depth (cm)	^{14}C Age (years BP)	Calibrated Age (cal. years BP)	Error (+/- years)
345	4810	3980	15
481	7030	6630	20
535	7120	6760	35
651	7400	7090	20

Table 3.1: ^{14}C ages from 4 depths, calibrated ages, and associated error.

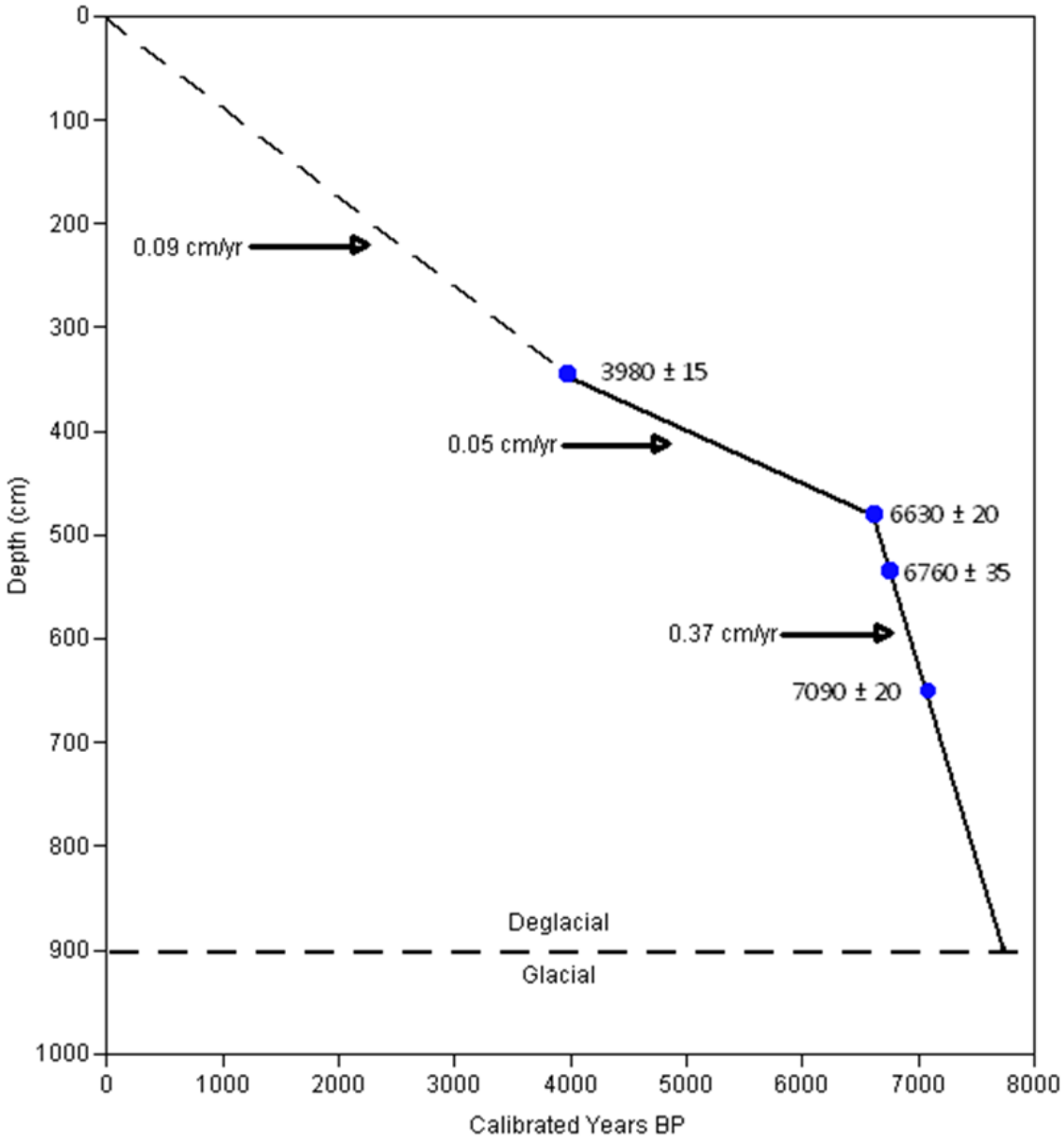

Figure 3.3: Age model and calculated sedimentation rates based on calibrated ^{14}C ages from 4 depths (after Smith, unpublished 2014).

Isotope Analysis:

Stable-oxygen isotope values were determined for samples with sufficient biogenic calcium carbonate to yield a result. Analysis of both benthic and planktonic foraminifera gives $\delta^{18}O$ values for both bottom-and surface-water masses, respectively (Figure 3.4). $\delta^{18}O$ values were obtained for 34 of the 92 samples, resulting in a discontinuous record. No $\delta^{18}O$ values were obtained above 211 cm due to the low abundance of calcareous foraminifera. $\delta^{18}O$ values ranged from 3.0 to 4.3 ‰. The bottom 2 m of the core has higher $\delta^{18}O$ values (>3.9 ‰). Between 200 and 800 cm the values range from 3.2 to 4.0 ‰. Above 400 cm the values decrease overall, with a range between 3.5 and 3.7 ‰.

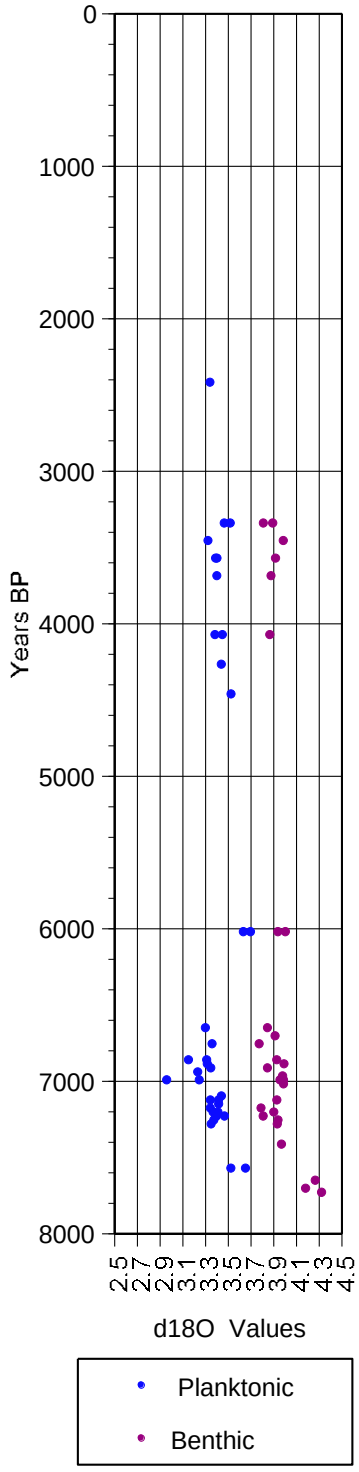

Figure 3.4: $\delta^{18}O$ values for planktonic (blue) and benthic (purple) foraminifera.

CHAPTER 4

DISCUSSION

Calcareous Foraminifera:

Fursenkoina spp. is the most abundant calcareous benthic foraminifer found in this study (Figure 4.1). It is often found along with other calcareous foraminifera including *Globocassidulina* spp., *N. iridea*, and the planktonic *N. pachyderma*. An assemblage dominated by *Fursenkoina* spp. was identified by Ishman and Domack (1994) in the Bransfield and Gerlache Straits. Both assemblages contain a majority of calcareous benthic foraminifera including *Fursenkoina* spp., *Globocassidulina* spp., and *Nonionella* spp. (Fig. 4.1). Ishman and Domack (1994) found this assemblage to have the same spatial distribution as the Weddell Sea Transitional Water (WSTW), which occupies the Bransfield Strait and adjacent areas including the Gerlache Strait. Modern assemblages dominated by *Fursenkoina* spp. have also been associated with less saline waters such as the Ice Shelf Water (ISW) or the Bransfield Strait Water (Anderson, 1975; Ishman and Szymcek, 2003). Other species found along with *Fursenkoina* spp. in these water masses are *Globocassidulina* spp. and *N. iridea*, which have also been associated with the ISW (Anderson, 1975; Ishman and Szymcek, 2003). These water masses are lower in salinity and less corrosive to the calcareous tests, which characterize the assemblages (Symcek et al., 2007; Milam and Anderson, 1985).

Fursenkoina spp. has been shown to occupy high productivity and low-oxygen environments, including the fjords of western AP (Alve, 1995; Ishman and Domack, 1994). *F. fusiformis* is the most abundant species in the fjords of northwest Europe, where estuarine

circulation results in stratification of the water column, high primary productivity, and oxygen-depleted bottom waters (Alve, 1990; Alve, 2002). *F. fusiformis* is also abundant in estuaries in eastern Canada (Scott et al., 1980; Miller et al., 1982). Alve (2002) suggests that the opportunistic behavior of *Fursenkoina* spp. causes it to be highly adapted to environmental stress in general, and not just to oxygen-depleted environments.

Ishman and Sperling (2002) identified an *F. fusiformis* assemblage in the Holocene record of the Palmer Deep. They interpreted high abundances of *F. fusiformis* in the early Holocene as opportunists taking advantage of the high organic flux caused by intense spring diatom blooms during ice-shelf retreat between 11,600 and 9000 years BP. Szymcek et al. (2007) interpreted a Holocene *F. fusiformis* assemblage to be indicative of ISW production caused by glacial melting in the Vega drift before 7000 years BP. Majewski and Anderson (2009) identify a *Globocassidulina* spp.-*F. fusiformis* assemblage in the Holocene record of the Firth of Tay. Their assemblage was dominated by *G. subglobosa* and is interpreted to be the most glacier-proximal assemblage, thriving in the coarse-grained glacial sediment following deglaciation between 9400 and 8300 years BP.

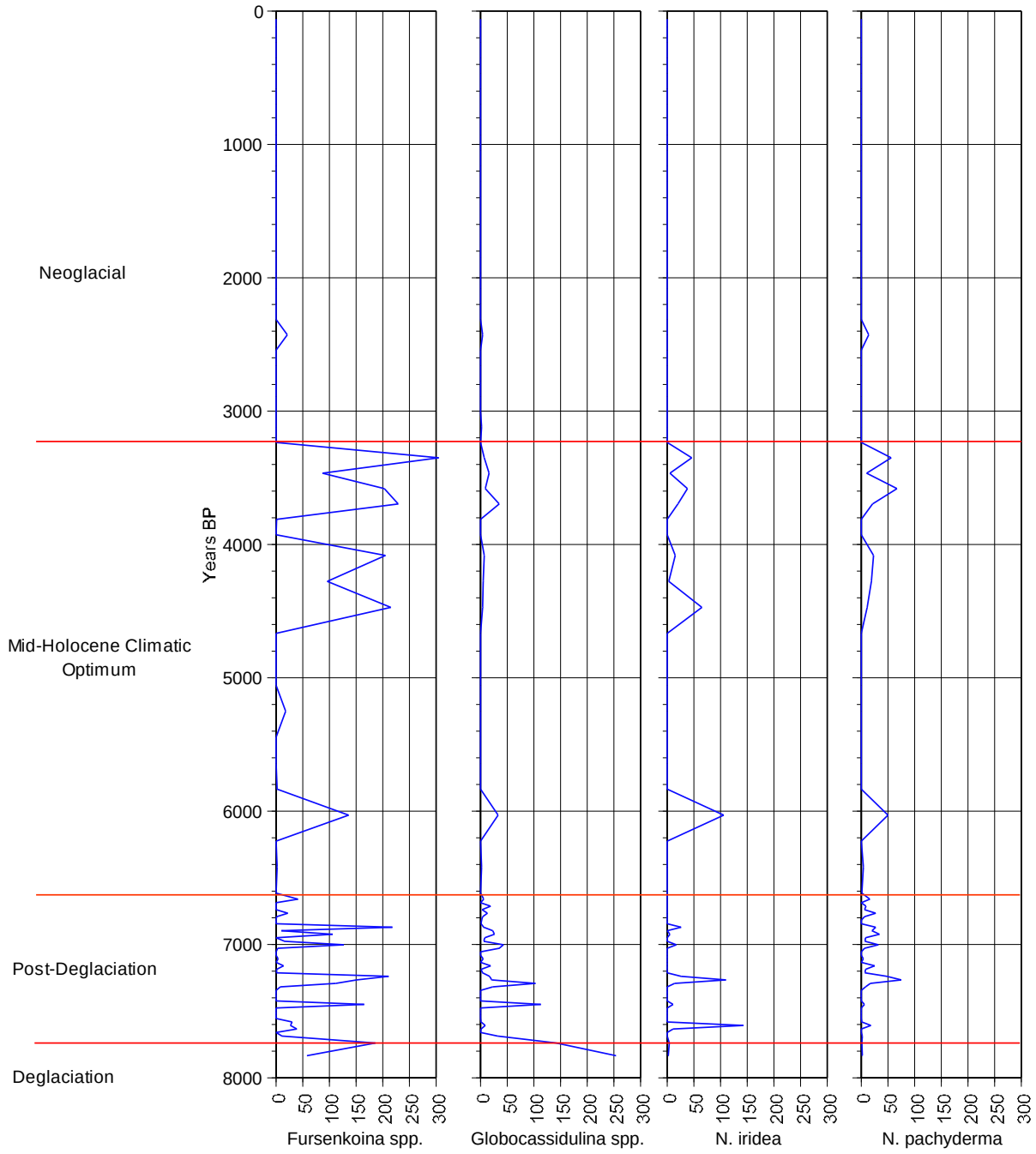

Figure 4.1: Abundance per sample of the most common calcareous foraminifera in this study*;* *Fursenkoina* spp.*, Globocassidulina* spp., *N. iridea*, and *N. pachyderma*.

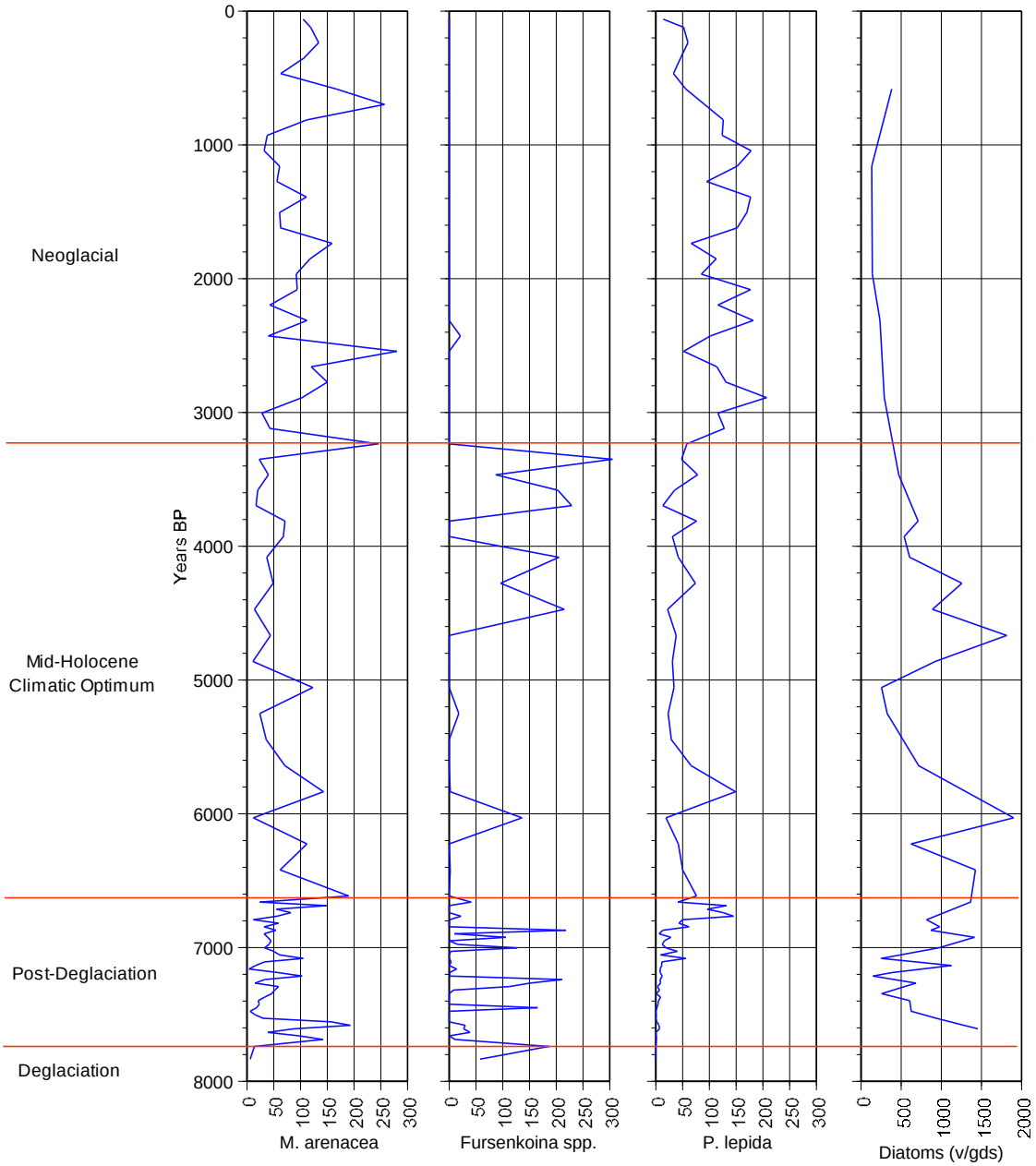

Figure 4.2: Total abundance per sample of the three most abundant foraminifera in this study*; M. arenacea*, *Fursenkoina* spp., and *P. lepida*. Diatom abundance is in v/gds (Diatom abundance data unavailable before 7610 ± 20 cal. years BP).

Agglutinated Foraminifera:

M. arenacea is the most abundant species in this study (Figure 4.2). It is most commonly found with other abundant agglutinated species but also occurs with calcareous species. A similar assemblage identified by Anderson (1975) is the Shallow Water Arenaceous Facies, located on the southwestern margin of the AP. Both of these assemblages include *M. arenacea*, *P. antarctica*, *Rhabdammina spp*., *Adercotryma glomeratum*, and *T. wiesneri*. Anderson (1975) found this assemblage in the presence of Saline Shelf Water (SSW) and suggested that the dominance of agglutinated forms is due to low preservation potential and carbonate dissolution caused by the cold, saline water mass. *M. arenacea* has been found in modern environments in the presence of Hyper Saline Shelf Water (HSSW) in the Prince Gustav Channel and in the Weddell Sea (Anderson, 1975; Ishman and Szymcek, 2003). *M. arenacea* has a high preservation potential, which is not affected by carbonate saturation or redox conditions (Schmeidl et. al., 1997). High abundances of M. arenacea are also associated with elevated ice conditions in the Ross Sea (Osterman and Kellogg, 1979).

Ishman and Sperling (2002) identified an assemblage dominated by *M. arenacea* in the Palmer Deep during the mid-Holocene. They suggested that the dominance of *M. arenacea* in the Palmer Deep during this time was due to its high preservation potential in the presence of the cold, corrosive HSSW. Szymcek et al. (2007) identified a nearly monospecific assemblage dominated by *M. arenacea*, which was interpreted as glacial production of HSSW. Majewski and Anderson (2009) identify an *M. arenacea* assemblage that becomes dominant in the Firth of Tay after 7750 years BP. This assemblage is more glacier-distal than the *F. fusiformis* assemblage from

the same study and is associated with higher primary productivity and more corrosive bottom waters during the MHCO.

P. lepida is the second most common foraminifer found in this study (Fig 4.2). High abundances of *P. lepida* are accompanied in almost all samples by other agglutinated foraminifera including *P. antarctica*, *S. biformis*, and *Rhumblerella* sp. This assemblage is similar to the southwestern continental shelf assemblage identified by Anderson (1975), which was found in areas with perennial ice cover and HSSW, where carbonate dissolution is the main factor controlling species distribution. Szymcek et al. (2007) also identify a Holocene assemblage dominated by additional agglutinated species besides the common *M. arenacea*. This assemblage was dominated by *Textularia wiesneri* and also included *M. arenacea*, *Portatrochammina* spp., and *S. biformis*. An increase in the *T. wiesneri* assemblage near the top of the core was interpreted as the taphonomic disintegration of agglutinated species besides *M. arenacea* down-core. Majewski and Anderson (2009) identify an assemblage dominated by two agglutinated species, *P. bartrami* and *P. antarctica*. *P. bartrami* is very similar to *P. lepida*, which shares the genus *Paratrochammina*. The *P. bartrami-P. antarctica* assemblage becomes dominant in the Firth of Tay after 3550 years BP and is interpreted to represent the cooler Neoglacial period and increasingly glacier-distal conditions as a result of a decrease in precipitation.

Deglaciation (7960 to 7740 ± 20 cal. years BP):

Sediment deposited between 7960 and 7830 ± 20 cal. years BP consists of a laminated mud overlain by pea-sized gravel that grades upward into sand. Beginning at 7830 ± 20 cal. years BP, a sequence of laminated rythmites are present until 7740 ± 20 cal. years BP. Graded sediments are consistent with turbidite deposits proximal to the ice-shelf grounding line (Bianchini, unpublished 2014; Christ et al., 2014). Foraminifera appear at 7830 ± 20 cal. years BP, and calcareous forms are dominant until 7690 ± 20 cal. years BP. At 7830 ± 20 cal. years BP the dominant species is *Globocassidulina* spp., accounting for 78 % of the total abundance (Figure 4.3). The next most abundant species at 7830 ± 20 cal. years BP is *Fursenkoina* spp. (17%). Both *Globocassidulina* spp. and *Fursenkoina* spp. are opportunistic species often found in environments of rapid environmental change *(*Alve, 2002; Anderson and Majewski, 2009). *Globocassidulina* spp. is also a glacier-proximal indicator, and its abundance in this interval is likely a response to recent ice-shelf retreat (Majewski, 2010). *Fursenkoina* spp. is known to occupy environments of intense spring diatom blooms that result in high organic flux to the sea floor (Alve, 2002). *Fursenkoina* spp. abundance at 7830 ± 20 cal. years BP is likely an opportunistic response to glacial retreat, and not to high organic content, because diatoms do not appear in the record until 7740 ± 20 cal. years BP. At 7740 ± 20 cal. years BP the most abundant species is *Fursenkoina* spp. (52 %), followed by *Globocassidulina* spp. (40 %). The appearance of diatoms in this interval indicates elevated primary productivity due to decreased glaciation. Longer periods of open-water conditions led to intense spring diatom blooms, causing elevated organic content in sea-floor sediments and an increase in abundance of *Fursenkoina* spp. Elevated *Fursenkoina* spp. abundance may also be a response to the presence of the less saline ISW

generated by the melting of sea ice. High *Globocassildulina* spp. abundance indicates that this is still a glacier-proximal environment, but with increasingly open-water conditions.

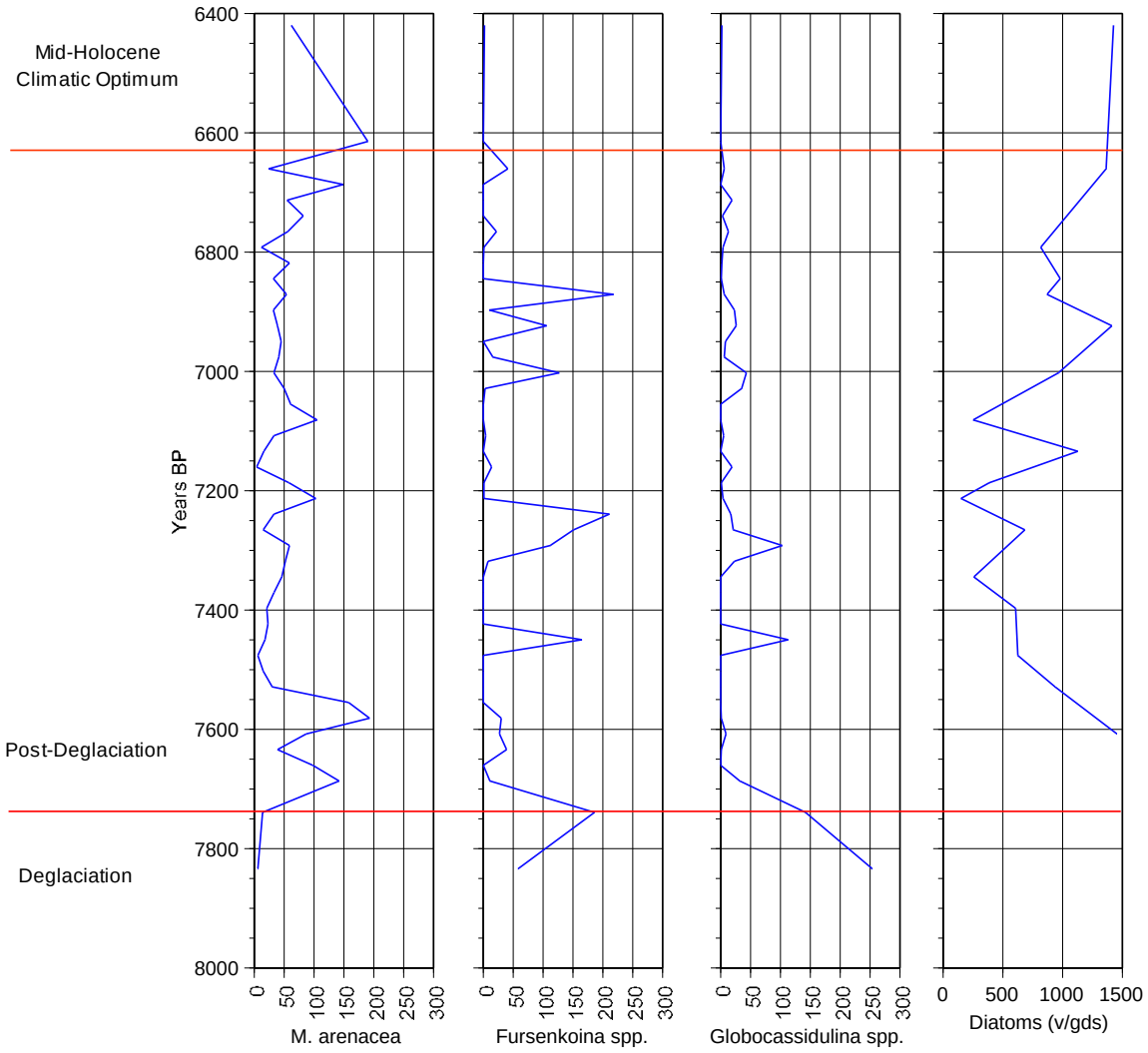

Figure 4.3: Abundances per sample of *M. arenacea*, *Fursenkoina* spp.*, Globocassidulina* spp., and diatoms (v/gds) until 6400 ± 20 cal. years BP.

Deglaciation of the Gerlache Strait is also indicated by $\delta^{18}O$ values from the benthic foraminifera (Figure 4.4). Benthic foraminifera at 7830, 7740, and 7690 ± 20 cal. years BP have $\delta^{18}O$ values of 4.3, 4.2, and 4.3 ‰, respectively. These three $\delta^{18}O$ values are heavier than any from benthic foraminifera from the rest of the core, which averages 3.9 ‰. Shackleton (1987) gives $\delta^{18}O$ values from 7 different cores from interglacial stage 1 (Holocene) that range from 3.11 to 3.38 ‰, with greater values, 4.92 to 5.25 ‰, in the preceding glacial stage 2. Based on the elevated $\delta^{18}O$ values, these samples appear to be a transitional state between glacial and interglacial periods. A decrease in $\delta^{18}O$ values during this time is likely caused by input of isotopically light water into the water column due to the melting of sea-ice. Current chronologies based on radiocarbon dates put the deglaciation of the Gerlache Strait some time before 8000 cal. years BP (Harden et al., 1992). Based on the age model for JPC-3, we put deglaciation at approximately ~7700 cal. years BP.

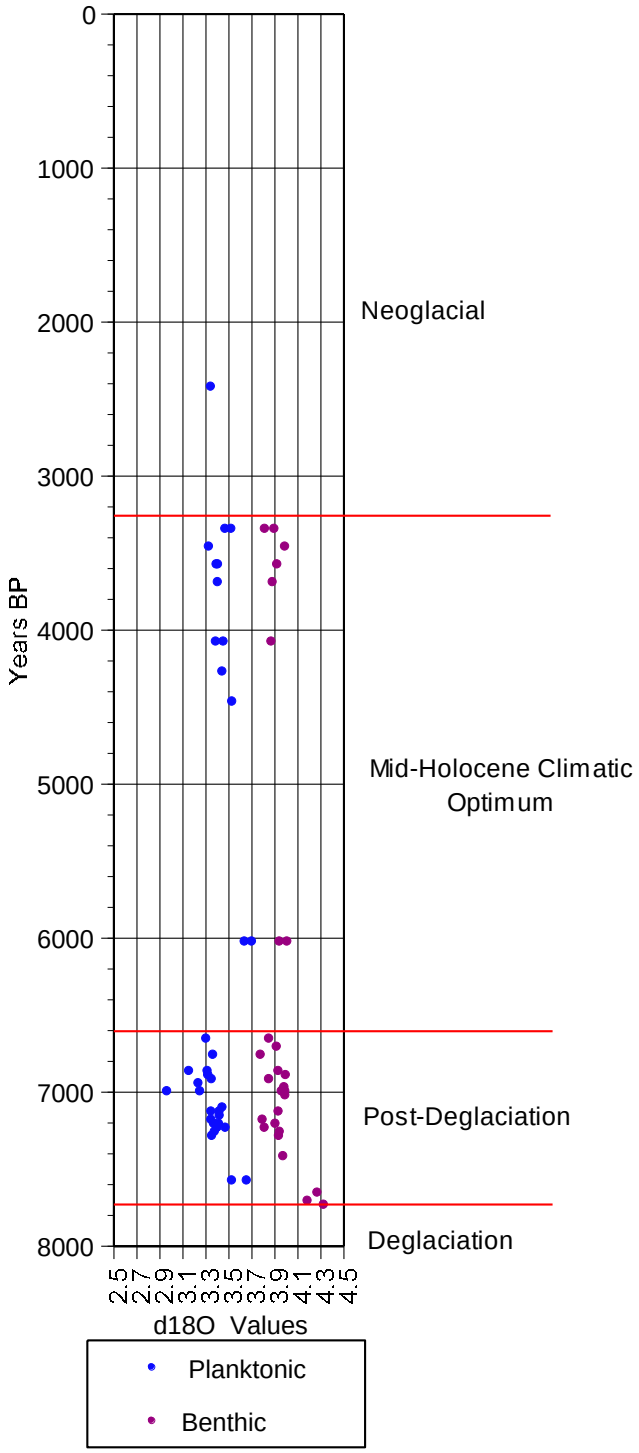

Figure 4.4: $\delta^{18}O$ values of planktonic *N. pachyderma* (blue) and benthic *Globocassidulina* spp. (purple).

Post-Deglaciation (7740 to 6630 ± 20 cal. years BP):

During the post-deglaciation period, foraminiferal assemblages in the study core alternate between *Fursenkoina* spp. -and *M. arenacea*-dominated on a scale of decades to centuries (Fig. 4.3). This is likely a response to variation in glacial conditions caused by relatively rapid environmental change, as the climate continues to transition from the LGM to the MHCO. *Globocassidulina* spp. averages 7 % and reaches 34 % abundance during this interval. High abundance of *Globocassidulina* spp. during this period indicates that the study area continued to be glacier-proximal. Higher sedimentation rates (0.38 cm/yr) also suggest a glacial depositional environment (Christ et al., 2014). Due to the proximity to the ice shelf, slight retreats or readvances would have led to changes in glacial conditions, influencing water mass characteristics and foraminiferal assemblages. Abundance of *M. arenacea* is likely a response to an increase in glacial conditions or seasonal sea-ice coverage. This would reduce primary productivity and increase the influence of HSSW in the Gerlache. Glacial melting and decreased seasonal sea ice would lead to increased primary productivity and greater influence of the ISW. Under these conditions the opportunistic *Fursenkoina* spp. is dominant. Other calcareous species are also more abundant during periods of production of the less corrosive ISW.

Beginning at 7690 ± 20 cal. years BP, sediments from core JPC-3 are characterized by alternating intervals of homogeneous and laminated diatom mud. Lamination of the sediments occurs during periods when bioturbation is absent due to high energy at the sea floor, high sedimentation rates, or anoxia. Wilmott et al. (2007) suggest that the southern end of the Gerlache Strait was blocked by ice during the middle Holocene, resulting in estuarine circulation. Bianchini (unpublished, 2014) found diatom abundances to be variable, but mostly elevated

during this interval. The proportion of the diatom *Chaetoceros* resting spores to vegetative cells was high, indicating high primary productivity (Crosta et al., 1997; Leventer et al., 2002; Bianchini, unpublished 2014). High abundance of *Chaetoceros* resting spores have also been associated with stratification of the water column (Crosta et al., 1997, Sjunneskog & Taylor, 2002; Bianchini, unpublished 2014). High primary productivity and water-column stratification are consistent with estuarine conditions. Bianchini (unpunished, 2014) also found high abundances of *F. kerguelensis* (~10 %) and *T. antarctica* (~30 %), both indicators of seasonally ice-free water (Crosta et al., 2005; Pike et al., 2009; Bianchini, unpublished 2014). *Eucampia* was found to have a long chain length, indicating short periods of winter sea-ice cover (Bianchini, unpublished 2014).

The stable-oxygen isotope record for the Post-Deglaciation period shows a difference in $\delta^{18}O$ values between benthic and planktonic foraminifera (Fig. 4.4). From 7630 ± 20 to 6660 ± 20 cal. years BP the $\delta^{18}O$ values from the benthic *Globocassidulina* spp. range from 3.8 to 4.3 ‰ and average 4.0 ‰. During the same interval, the $\delta^{18}O$ values from the planktonic foraminifer *N. pachyderma* range from 3.0 to 3.7 ‰ and average 3.4 ‰. The difference in average $\delta^{18}O$ values between benthic and planktonic foraminifera is 0.6 ‰.

When comparing $\delta^{18}O$ values of different species, it is important to consider whether a metabolic vital effect in some species causes calcium carbonate to precipitate in disequilibrium with ambient water. Norris et al., (1998) found that the *N. pachyderma* precipitates calcium carbonate with $\delta^{18}O$ values close to those of calcium carbonate precipitated in equilibrium with seawater. Norris et al., (1998) also found that both the surface water and *N. pachyderma* were isotopically lighter the nearer they were to the ice shelf in the Weddell Sea. Benthic foraminifera have been known to precipitate calcium carbonate in disequilibrium with seawater due to a vital

effect or habitat preferences (Duplessy et al., 1970; McCorkle et al., 1990). *G. subglobosa* has been shown to have $\delta^{18}O$ values that are isotopically lighter by 0.52 ‰ than calcium carbonate precipitated in equilibrium (Graham et al., 1981). This effect has not been corrected for in the data, but would essentially double the difference in isotope ratios between benthic and planktonic foraminifera.

This difference in isotope ratios between the benthic and planktonic calcium carbonate is indicative of a stratified water column. It is unlikely that the difference in isotope ratios in this case is a signal of temperature. During the Holocene, the surface and bottom water of the Antarctic would both be close to freezing, so a difference in $\delta^{18}O$ values is more likely a result of salinity stratification (Norris et al., 1998; Domack et al., 2005). Elevated seasonal glacial and sea-ice melt would have introduced a flux of isotopically light freshwater into the water column. Blockage of the southern opening of the Gerlache Strait would have resulted in reduced communication between the waters of the Gerlache and the primary continental-shelf water masses. Reduced mixing with shelf waters would have led to the formation of fresher surface water and a denser, more saline bottom water. This type of stratification is common in estuarine circulation regimes (Wilmott et al., 2007).

Mid-Holocene Climatic Optimum (6630 ± 20 to 3240 ± 15 cal. years BP):

The beginning of MHCO in the Gerlache Strait is marked by a sudden decrease in sedimentation rates, from 0.38 cm/yr before 6630 ± 20 cal. years BP to 0.053 cm/yr. A change in foraminiferal assemblages also occurs at this point, with a shift towards more stable and consistent dominance of agglutinated species *M. arenacea* and *P. lepida* until 4470 ± 20 cal. years BP (Fig. 4.2). During this period, *M. arenacea* averages 45 % of total abundance and reaches up to 65 %. *P. lepida* averages 35 % total abundance and reaches 65 %. *Fursenkoina* spp. and other calcareous species are almost entirely absent, except for individual samples (Fig. 4.2). During the post-deglaciation phase and the onset of the MHCO, glacial conditions were unstable, resulting in high-frequency variation in foraminiferal assemblages during that time. Once the MHCO was established in the Strait, the ice sheets would have stabilized nearer to the coastline, farther from the JPC-3 core site. This shift to a more stable agglutinated assemblage suggests a more persistent occupation of the outer portion of the Gerlache by HSSW (Anderson, 1975). *M. arenacea* has also been associated with the MHCO on the AP shelf and its sustained abundance beginning at 6630 ± 20 cal. years BP is interpreted here to indicate the onset of the MHCO in the Gerlache Strait.

Because of the presence of corrosive HSSW in the Strait between 6630 and 4470 ± 20 cal. years BP, calcareous species are rare, and stable isotope data is incomplete. One sample within this interval contained sufficient calcium carbonate to yield $\delta^{18}O$ values. At 6030 ± 20 cal. years BP there is a difference in $\delta^{18}O$ values between benthic (4.0 ‰) and planktonic species (3.6, 3.7 ‰), however it is not possible to draw conclusions for this entire interval based on one sample. It is likely, however, that stratification and estuarine circulation conditions remained during this

time, based on lamination of the sediments. Dominant species at 6030 ± 20 cal. years BP include *Fursenkoina* spp. (33 %), *Globocassidulina* spp. (8 %), and the planktonic *N. pachyderma* (12 %). Abundance of calcareous species in this sample indicates a period of increased influence of ISW. High abundance of *N. pachyderma*, as well as high diatom abundance indicates high primary productivity. *Globocassidulina* spp. indicates a more glacier proximal environment. Prior to this interval the ice shelves may have advanced nearer to the study location, then began retreating again. This would result in production of the ISW near the study location, causing a high abundance of the opportunistic *Fursenkoina* spp., the glacier proximal *Globocassidulina* spp., and elevated primary productivity.

After 6030 ± 20 cal. years BP, a decline in diatom abundance suggests a glacial readvance. The foraminiferal assemblage continues to be dominated by agglutinated taxa, but with a decrease in total abundance. This mid-Holocene glaciation ends at 4470 ± 20 cal. years BP, when *Fursenkoina* spp. becomes the most abundant species. During this interval *Fursenkoina* spp. ranges from 28 % to 61 % of total abundance, except for 2 consecutive samples (3930 and 3810 ± 15 cal. years BP) where abundances are 0 % to 0.5 %. This interval, except for the two calcareous-depleted samples, is abundant in other calcareous foraminifera including *Globocassidulina* spp. (1-9 % total abundance), *N. iridea* (1-17 %), and *N. pachyderma* (3-10 %). Because of the abundance of multiple calcareous species, this assemblage is likely a response to presence of the ISW and glacial retreat. *Fursenkoina* spp. abundance is also likely a response to high primary productivity, indicated by high abundance of diatoms and the planktonic *N. pachyderma*.

The elevated influence of ISW in the Gerlache between 4470 ± 20 and 3350 ± 15 cal. years BP is also likely a response to enhanced estuarine conditions, similar to those seen in the Post-Deglaciation period. Because calcareous species are common, $\delta^{18}O$ values are available, and suggest estuarine conditions (Fig 4.4). During this interval, $\delta^{18}O$ values from benthic foraminifera range from 3.8 to 4.0 ‰, and average 3.9 ‰, with $\delta^{18}O$ values from planktonic foraminifera range from 3.3 to 3.5 ‰ and average 3.4 ‰. Continued lamination of sediments in this interval also provides evidence for water-column stratification and estuarine circulation.

Neoglacial (3240 ± 15 cal. years BP to present):

Beginning at 3240 ± 15 cal. years BP, foraminiferal assemblages are again dominated by agglutinated species (Fig. 4.1) *M. arenacea* is abundant, ranging from 11 % to 65 % total abundance, and averaging 34 % abundance. *P. lepida* also becomes abundant in the top interval, ranging from 7 % to 6 3% total abundance and averaging 35 %. Calcareous foraminifera are essentially non-existent in the top interval, suggesting the presence of a corrosive water mass that inhibits either precipitation or preservation of calcium carbonate (Fig. 4.2). Increased glaciation and seasonal sea-ice cover during the Neoglacial period would have led to the production of HSSW, which is known to prevent calcareous foraminifera from living or being preserved, while agglutinated species are able to thrive (Anderson, 1975). Estuarine conditions likely persisted for part of the Neoglacial, however the absence of calcareous foraminifera after 3240 ± 15 cal. years BP precludes $\delta^{18}O$ values. Laminated sediments continue until 2430 ± 15 cal.

years BP. After this time, sediments are homogeneous and bioturbated, likely indicating the end of a stratified water column and estuarine conditions.

Incursions of UCDW into the Palmer Deep during the Neoglacial are suggested by abundant *Bulimina aculeata* (Ishman and Domack, 1994; Ishman and Sperling, 2002). It is possible that contact with the warm UCDW would have melted sea ice blocking the southern passages to the Gerlache Strait, allowing for better communication with deeper shelf-water masses and less estuarine conditions. If the UCDW did cause any melting of sea ice in the southern Gerlache, then it did not reach as far north as the JPC-3 core site. A total of 18 *B. aculeata* were found in the entire core, indicating no significant presence of UCDW. Of the 18 total *B. aculeata* found, 10 were from a single sample, at 3350 ± 15 cal. years BP, which is our date for the end of the MHCO. Ishman and Sperling (2002) identify three incursion of UCDW into the Palmer Deep during the Neoglacial, the first beginning at 3400 years BP and lasting until 3000 years BP. They constrain the Neoglacial to 3700 years BP until present, which agrees with the timing found in this study.

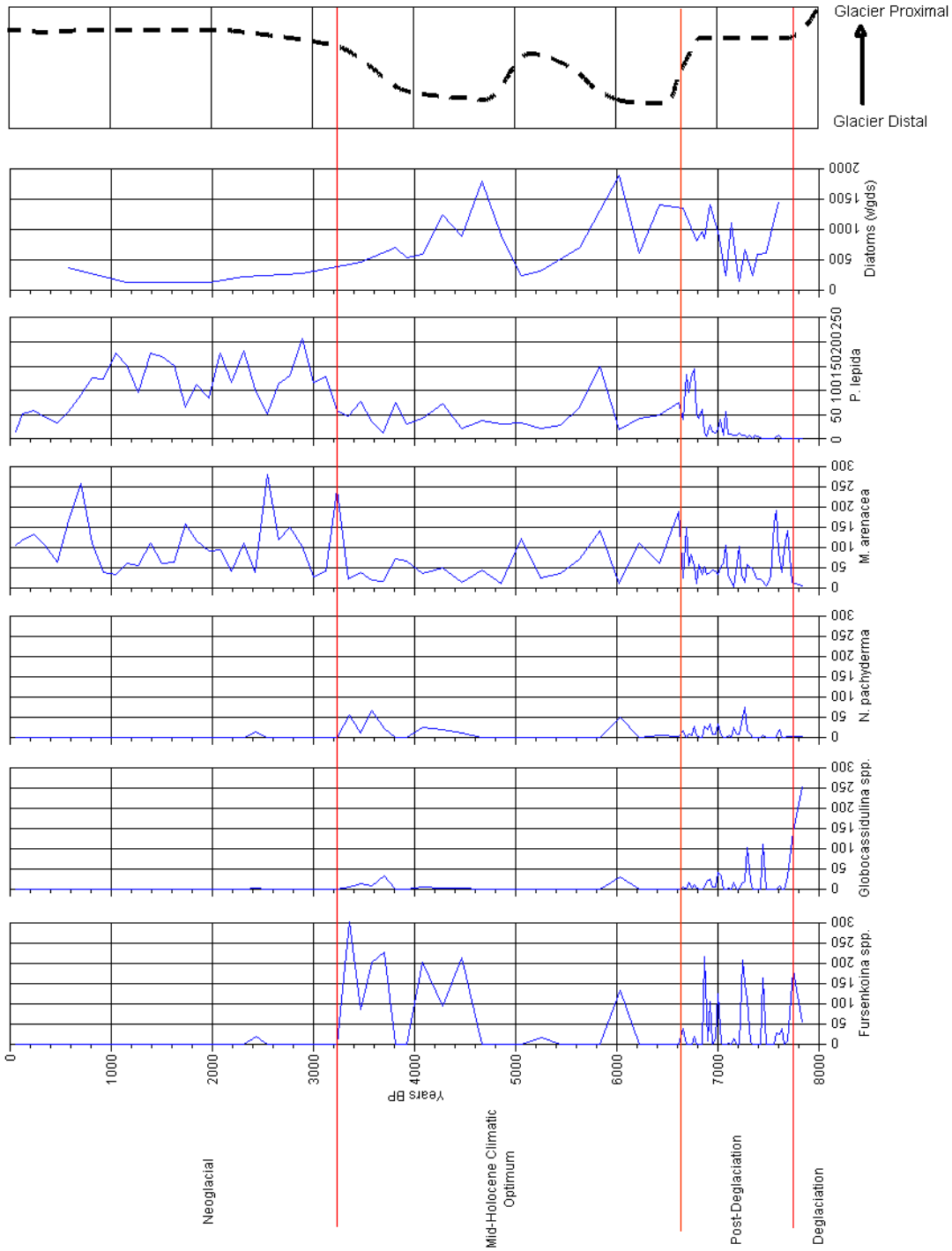

Figure 4.5: Summary figure with important foraminifera species abundance, diatom abundance, and the proximity the core site to the ice shelf.

CHAPTER 5

SUMMARY AND CONCLUSIONS

1) Abundance of the opportunistic *Fursenkoina* spp. and the ice-proximal *Globocassidulina* spp., accompanied by the appearance of diatoms, indicates that the JPC-3 core site had deglaciated by 7740 ± 20 cal. years BP. Evidence for deglaciation also includes enrichment of ^{18}O in benthic foraminifera until 7690 ± 20 cal. years BP. This timing for deglaciation is slightly later than, but consistent with previously reported ages of >8000 cal. years BP for deglaciation of the Gerlache Strait (Harden et al., 1992).
2) Rapidly alternating dominance of *Fursenkoina* spp. and *M. arenacea* following deglaciation indicates a period of glacial instability. The study site remained glacier-proximal during this time, and small retreats and readvances of the ice shelf would have produced alternating influence of ISW and HSSW. Glacier-proximal conditions are also evident by the abundance of *Globocassidulina* spp.
3) The difference in $\delta^{18}O$ values between benthic and planktonic foraminifera is interpreted as a stratified water column during the Post-Deglaciation period. Stratification is also evident by high primary productivity, *Fursenkoina* spp. abundance, and laminated sediments. A stratified water column may be the result of enhanced estuarine conditions caused by the blockage of the southern Gerlache Strait by ice, as suggested by Wilmott et al. (2007).
4) The beginning of the MHCO at 6630 ± 20 cal. years BP is marked by a decrease in sedimentation rates and a shift to an agglutinated foraminiferal assemblage dominated

by *M. arenacea* and *P. lepida*. A shift to agglutinated foraminifera suggests more persistent HSSW in the Gerlache. *M. arenacea* is associated with the MHCO, and together with *P. lepida,* represents more glacier-distal assemblage (Majewski and Anderson, 2009).

5) A period of glacial re-advance occurs during the MHCO after 6030 ± 20 cal. years BP, indicated by a decline in diatom abundances. This period lasts until 4470 ± 20 cal. years BP when calcareous taxa become abundant and ISW becomes the dominant water mass.
6) During the MHCO, from 4470 ± 20 to 3350 ± 15 cal. years BP, estuarine conditions are once again persistent. A shift back to the *Fursenkoina* spp.-dominated assemblage suggests the presence of ISW and high primary productivity. Laminated sediments and depletion of ^{18}O in planktonic foraminifera suggests stratification of the water column associated with estuarine circulation.
7) The beginning of the Neoglacial at 3240 ± 15 cal. years BP is marked by a shift back to an *M. arenacea*-and *P. lepida*-dominated assemblage. During this period, agglutinated taxa are dominant, while calcareous forms are almost entirely absent, suggesting persistent HSSW.
8) Estuarine circulation may have continued into the Neoglacial, but its influence is uncertain due to the absence of calcareous foraminifera and associated $\delta^{18}O$ values. Lamination of the sediment continues until 2430 ± 15 cal. years BP, likely indicating the end of water-column stratification and the end of estuarine conditions.

9) Absence of *B. aculeata* from this core indicates that the UCDW never occupied this portion of the Gerlache Strait. Because *B. aculeata* was abundant in the adjacent Palmer Deep during the Neoglacial, its absence provides further evidence for the blockage of the southern Gerlache Strait by ice. Incursion of the warm UCDW into the Palmer Deep during the Neoglacial may also have resulted in the melting of sea ice blocking the southern Gerlache, leading to the eventual reduction in estuarine conditions.

REFERENCES

Alve, E., 1995, Benthic foraminiferal distribution and recolonization of formerly anoxic environments in Drammensfjord, Southern Norway: Marine Microplaeontol., 25, p. 169-186.

Alve, E. A., 2002, Common opportunistic foraminiferal species as an indicator of rapidly changing conditions in a range of environments: Estuarine, Coastal and Shelf Sci. 57, p. 501–514.

Anderson, J.B., 1975, Ecology and distribution of foraminifera in the Weddell Sea of Antarctica: Micropaleontology, 21, p. 69–96.

Anderson, J.B., 1999, Antarctic marine geology: Cambridge University Press.

Brady, H. B., 1878, On the reticularian and radiolarian Rhizopoda (Foraminifera and Polycystina) of the North Polar Expedition of 1875–76: Annals and Magazine of Natural History, 5, 1, p. 425–440.

Brady, H. B., 1879, Notes on some of the reticularian Rhizopoda of the ‘‘Challenger’’ Expedition. Part 1. On new or little-known arenaceous types: Quarterly Journal of Microscopic Sciences, new series, 19, p. 20–63.

Banfield, L. A., and Anderson, J. B., 1995, Seismic facies investigation of the late quaternary glacial history of Bransfield Basin, Antarctica: geology and seismic stratigraphy of the Antarctic margin: Antarctic Research Series, 68, p. 123-140.

Barcena, M. A., R. Gersonde, S. Ledesma, J. Fabres, A. M. Calafat, M. Canals, J. Sierro, and J. A. Flores, 1998, Record of Holocene glacial oscillations in Bransfield Basin as revealed by siliceous microfossil assemblages: Antarct.Sci., 10, p. 259– 285.

Barker, P.F., Barrett, P.J., Cooper, A.K., Huybrechts, P., 1999, Antarctic glacial history from numerical models and continental margin sediments: Palaeogeography, Palaeoclimatology, Palaeoecology. 150, p. 247-267.

Bentley, M. J., and Anderson, J. B., 1998, Glacial and marine geological evidence for the ice sheet configuration in the Weddell Sea-AP region during the last glacial maximum: Antarctic Science, 10, p. 309–325.

Berger, W.H., 1979, Stable Isotopes in Foraminifera: Foraminiferal Ecology and Paleoecology, p. 156-198.

Bianchini, A.M., 2014, Reconstruncting Holocene paleoclimate in the Gerlache Strait, West AP. Unpublished undergraduate thesis, Colgate University.

Bindschandler, R., 2006, The environment and evolution of the West Antarctic ice sheet: setting the stage: Philosophical Transactions of the Royal Society A: Mathematical, Physical and Engineering Sciences, 364, p. 1583-1605.

Brachfeld, S., Domack, E.W., Kissel, C., Laj, C., Leventer, A., Ishman, S., Gilbert, R., Camerlenghi, A. and Eglinton, L., 2003, Holocene history of the Larsen-A Ice Shelf constrained by geomagnetic paleointensity dating: Geology, 31, p. 749–52.

Bronnimann, P., and Whittaker, J. E., 1980, A redescription of Trochammina nana (Brady) (Protozoa: Foraminiferida), with observations on several other Recent Trochammininidae in the collections of the British Museum (Natural History): Bulletin of the British Museum (Natural History). Zoology series, 38, 4, p. 175–185.

Capella, J.E., Ross, R.M., Quetin, L.B., and Hofmann, E.E., 1992, A note on the thermal structure of the upper ocean in the Bransfield Strait-South Shetland Islands region: Deep-Sea Research I, 39, p. 1221–1229.

Canals, M., Estrada, F., Urgeles, R. and GEBRAP Team. 1998, Very high-resolution seismic definition of glacial and postglacial sediment bodies in the continental shelves of the northern Trinity Peninsula region, Antarctica: Ann. Glaciol., 27, p. 260–264.

Canals, M., Urgeles, R., and Calafat, A.M., 2000, Deep sea-floor evidence of past ice streams off the AP: Geology, 28, p. 31–34.

Canals, M., Casamor, J.L., Urgeles, R., Calafat, A.M., Domack, E.W., Baraza, J., Farran, M., and De Batist, M., 2002, Seafloor evidence of a subglacial sedimentary system off the northern AP: Geology 30, p. 603–606.

Ciais, P., Petit, J.R., Jouzel, J., Lorius, C., Barkov, N.I., Lipenkov, V.and Nicolaïev, V., 1992, Evidence for an early Holocene climatic optimum in the Antarctic deep ice-core record: Climate Dynamics, 6, p. 169–77.

Coplen T. B. (1996) New guidelines for reporting stable hydrogen, carbon, and oxygen isotope-ratio data. Geochim. Cosmochim. Acta 60, 3359–3360.

Crosta, X., Pichon, J., and Labracherie, M., 1997, Distribution of *Chaetoceros* resting spores in modern peri-Antarctic sediments: Marine Micropaleontology, 29, p. 283-299.

Crosta, X., Romero, O., Armand, L. K., and Pichon, J., 2005, The biogeography of major diatom taxa in Southern Ocean sediments: 2. Open ocean related species, Palaeogeography, Palaeoclimatology, Paleoecology, 223, p. 66-92.

Davies, Bethan J., Hambrey, Michael J., Smellie, John L., Carrivick, Jonathan L., and Glasser, Neil F., 2012, AP Ice Sheet evolution during the Cenozoic Era: Quaternary Science Reviews, 31, p. 30-66.

De Montfort, D. P., 1808, Conchyliologie syste´matique et classification me´thodique des coquilles: F. de Schoell, Paris, tome 1, p. 409.

Dennison, J. M., and Hay, W. W., 1967, Estimating the needed sampling area for subaquatic ecologic studies: J. Paleontol., 41, p.706-708.

Domack, E. W., and Mammone, K. A., 1993, Modern sedimentation within Andvord Bay, AP: Antarctic Journal of the United States, 28, p. 97–98.

Domack, E. W., and Leg 178 Scientific Party, 1998, Mysteries of the Pamer Deep Revealed: ODP Leg 178 to AP: Joint Oceanographic Institutuions/U.S. Science Advisory Committee Newsletter, 11, p. 8-11.

Domack, E. W., Leventer, A., Gilbert, R., Brachfield, S., Ishman, S., Camerlenghi, A., Gavahan, K., Carlson, D., and Barkoukis, A. 2001, Cruise reveals history of Larsen Ice Shelf: EOS, 82(2).

Domack, E.W. and McClennen, C.E., 1996, Accumulation of glacial marine sediments in fjords of the AP and their use as late Holocene palaeoenvironmental indicators. In Ross, R.M., Hofmann, E. and Quetin, L.B., editors, Foundations for ecological research west of the AP: Antarctic Research Series 70, American Geophysical Union, 135–54.

Domack, E.W., 2002, A synthesis for site 1098: Palmer Deep. In Barker, P.F., Camerlenghi, A., Acton, G.D. and Ramsay, A.T.S., editors, Proceedings of the ocean drilling program, scientific results: Ocean Drilling Program, Texas A&M University.

Domack E., Burnett A., and Leventer A., 2003, Environmental setting of the AP: Antarctic Research Series, 79, p. 1-13.

Domack E., Duran D., Leventer A., Ishman S., Doane S., McCallum S., Amblas D., Ring J., Gilbert R., and Prentice M., 2005, Stability of the Larsen B ice shelf on the AP during the Holocene epoch: Nature, 436, p. 681-685.

Domack, E., 2015, Unpublished radiocarbon data.

D'orbigny, A. D., 1826, Tableau me´thodique de la classe desCe´phalopodes: Annales des Sciences Naturelles, se´r. 1, tome 7, p. 245–314.

Dowdeswell, J.A., O´ Cofaigh, C., Pudsey, C.J., 2004, Continental slope morphology and sedimentary processes at the mouth of an Antarctic palaeo-ice stream: Marine Geology.

Duplessy, J. C., C. Lalou, and A. C. Vinot, 1970, Differential isotopic fractionation in benthic foraminifera and paleotemperatures reassessed, Science, 168, 250– 251.

Earland, A., 1934, Foraminifera. Part III. The Falklands sector of the Antarctic (excluding South Georgia): Discovery Reports 10, p. 1–208.

Eagles, G., Livermore, R. A., 2002, Opening history of Powell Basin, AP: Marine Geology, 185, p. 195-205.

Elliot, D.H., 1997, The planar crest of Graham Land, Northern AP: possible origins and timing of uplift: in Geology and Seismic Stratigraphy of the Antarctic Margin, 2.

Evans, J., Dowdeswell, J.A., and O´ Cofaigh, C., 2004, Late Quaternary submarine bedforms and ice-sheet flow in Gerlache Strait and on the adjacent continental shelf, AP: J. Quaternary Sci., Vol. 19, p. 397-407.

González-Casado, J. M., Giner-Robles, J. L., and López-Martínez, J., 2000, Bransfield Basin, AP: Not a normal baccal. karc basin Geology: 28, 11, p. 1043–1046.

Gordon, A.L.t D.T. Georgi, and Talor, H. W., 1977, Antarctic Polar Front zone in the western Scotia Sea-Summer 1975: J. Phys. Oceanogr., 7, p. 309-328.

Gordon, A. L., 1998, Western Weddell Sea thermohaline stratification: In S. S. Jacobs & R. F. Weiss, Interactions at the Antarctic continental margins: Antarctic Research Series, 75, p. 215–240.

Graham, D.W., Corliss, B. H., Bender, M. L., and Keigwin, L. D., 1981, Carbon and oxygen isotopic disequilibria of Recent deep-sea benthic foraminifera. Mar. Micropaleontol., 6, p. 483-497.

Harden, S.L., DeMaster, D.J. and Nittrouer, C.A., 1992, Developing sediment geochronologies for high-latitude continental shelf deposits: a radiochemical approach: Marine Geology, 103, p. 69–97.

Harris, Peter T., Domack, Eugene, Manley, Patricia L., Gilbert, Robert, and Leventer, Amy., 1999, Andvord Drift; a new type of inner shelf, glacial marine deposystem from the AP: Geology, 27, 8, p. 683-686.

Heron−Allen, E. and Earland, A., 1922, Protozoa. Part III – Foraminifera. British Antarctic (Terra Nova) expedition 1910: Natural History Report, Zoology, 6, p. 25–268

Hjort, C., Ingolfsson, O., Moller, P., and Lirio, J. M., 1997., Holocene glacial history and sea-ice changes on James Ross Island, AP: Journal of Quaternary Science, 12, p. 259-273.

Hjort,C ., Bentley,M . J., and Ingolfsson, 6., 2001, Holocene and pre-Holocene temporary absence of the George VI Ice Shelf, AP: Antarctic Science, 13. p. 296-301.

Hofmann, B.E., and T. Whitworth, III, 1985, A synoptic description of the flow through Drake Passage from year-long measurements: J. Geophys. Res., 90, p. 7177-7187.

Hofmann, E. E., and Klinck, J. M., 1998, Thermohaline variability of the waters overlying the West AP continental shelf, in Ocean, Ice, and Atmosphere: Interactions at the Antarctic Continental Margin: Antarct. Res. Ser., 75, edited by S. S. Jacobs, p. 67– 81.

Igarashi, Atsuo, Numanami, Hideki, Tsuchiya, Yasutacal. ka, and Fukuchi, Mitsuo. 2001, Bathymetric
distribution of fossil foraminifera within marine sediment cores from the eastern part of Lützow-Holm Bay, East Antarctica, and its paleoceanographic
implications: Marine Micropaleontology, 42, 3, p. 125-162.

Ingolfsson, Olafur, Hjort, Christian, and Humlum, Ole. 2003, Glacial and climate history of the AP since the Last Glacial Maximum: Arctic Antarctic and Alpine Research, 35, 2, p. 175-186.

Ishman, S. E., and Domack, E. 1994, Oceanographic controls on benthic foraminifers from the Bellingshausen margin of the AP: Marine Micropaleontology, 1994, 24, 2.

Ishman, S.E., and Sperling, M.R., 2002, Benthic foraminiferal record of Holocene deep-water evolution in the Palmer Deep, western AP: Geology, 30, p. 435-438.

Ishman, S.E., and Szymcek, P., 2003, Foraminiferal distributions in the former Larsen-A Ice Shelf and Prince Gustave Channel region, Eastern Antarctica Peninsula margin: A baseline for Holocene paleoenvironmental change, Environmental setting of the AP: Antarctic Research Series, 79, p. 239-260.

Kennett, J.P., 1967, New foraminifera from the Ross Sea, Antarctica: Contributions from the Cushman Foundation for Foraminiferal *Research* 18, 3, p. 133–135.

Kennett, J. P., Houtz, R., Andrews, P., Edwards, A., Gostin, V., Hajos, M., Hampton, M., Jenkins, D., Margolis, S., Ovenshine, A., and Perch-Nielsen, K., 1975, Cenozoic paleoceanography in the southwest Pacific Ocean, Antarctic glaciation, and the development of the Circum-Antarctic Current.

Khim, B., Yoon, H.I., Cal. kang, C.Y. and Bahk, J.J., 2002, Unstable climatic oscillations during the late Holocene in the eastern Bransfield Basin, AP: Quaternary Research, 58, p. 234–45.

Klinck, J. M., and Smith, D. A., 1993, Effect of wind changes during the Last Glacial Maximum on the circulation of the Southern Ocean: Paleoceanography, 8, p. 427– 433.

Laberg, Jan Sverre and Vorren, Tore O. 2004, Weichselian and Holocene growth of the northern high-latitude Lofoten Contourite Drift on the continental slope of Norway: Sedimentary Geology, 16, 1, p. 1-17.

Leventer, A., Domack, E. W., Ishman, S. E., Brachfield, S., McClennen, C. E., and Manley, P., 1996, Productivity cylcles of 200-300 years in the AP region: understanding lincal. kages among the sun, atmosphere, oceans, sea ice, and biota: Geological Society of America Bulletin, 108, p. 1642-1644.

Leventer, A., Domack, E. W., Barkoukis, A., McAndrews, and Murray, J., 2002, Laminations from the Palmer Deep: a diatom-based interpretation: Paleoceanography.

Leventer, A., 2015. Unpublished diatom and radiocarbon data.

McCorkle, D. C.; Keigwin, L. D.; Corliss, B. H. & Emerson, S. R., 1990, The influence of microhabitats on the carbon isotopic composition of deep-sea benthic foraminifera. Paleoceanography, 5, p. 161-185.

Milam, R.W., and Anderson, J.B., 1981, Distribution and ecology of Recent benthonic foraminifera of the Adelie-George V continental shelf and slope, Antarctica: Marine Micropaleontology, 6, p. 297–325.

Miller, A.A.L., Mudie, P.J., Scott, D.B., 1982, Holocene history of Bedford Basin, Nova Scotia: foraminifera, dinoflagellate and pollen records: Can. J. Earth Sci., 19, p. 2342-2367.

Majewski W. 2005. Benthic foraminiferal communities: distribution and ecology in Admiralty Bay, King George Island, West Antarctica: Polish Polar Research, 26, p. 159–214.

Majewski W. and Zajączkowski M. 2007. Benthic foraminifera in Adventfjorden, Svalbard: Last 50 years of local hydrographic changes: Journal of Foraminiferal Research, 37, p. 107–124.

Majewski, W., and Anderson, J.B., 2009, Holocene foraminiferal assemblages from Firth of Tay, AP: Paleoclimate implications: Marine Micropaleontology, 73, p. 135–247.

Majewski, W., 2010, Benthic foraminifera from West Antarctic fjord environments: An overview: Polish Polar Research, 31, p. 61-82.

Masson, V., Vimeux, F., Jouzel, J., Morgan, V., Delmotte, M., Ciais, P., Hammer, C., Johnsen, S., Lipenkov, V., Mosley-Thompson, E., Petit, J.R., Steig, E.J., Stievenard, M. and Vaikmae, R., 2000, Holocene climate variability in Antarctica based on 11 ice-core isotopic records: Quaternary Research, 54, p. 348–58.

Masson-Delmotte, V., Stenni, B. and Jouzel, J., 2004, Common millennial-scale variability of Antarctic and Southern Ocean temperatures during the past 5000 years reconstructed from the EPICA Dome C ice core: The Holocene, 14, p. 145–51.

Mosby, H., 1934, The waters of the Atlantic Antarctic Ocean: Sci. Res. Norw. Antarct. Exped. 1927-1928, 11, p. 1-131.

Norris, R. D., et al., 1998, Proceedings of the Ocean Drilling Program, Initial Reports, vol. 171B, 749 pp., Ocean Drill. Prog., College Station, Tex.

O´Cofaigh, C., Pudsey, C.J., Dowdeswell, J.A., Morris, P., 2002, Evolution of subglacial bedforms along a palaeo-ice stream, AP continental shelf: Geophysical Research Letters 29, 8.

Osterman, L.E., and Kellogg, T.B., 1979, Recent benthic foraminifer distributions from the Ross Sea, Antarctica: Relation to ecologic and oceanographic conditions: Journal of Foraminiferal Research, 9, p. 250–269.

Parr, W. J., 1950, Foraminifera. *B.A.N.Z. Antarctic Research Expedition 1929–1931, Report*, Series B, 5, 6, p. 232–392, pls. 3–15.

Parker, W. K., and JONES, T. R., 1865, On some Foraminifera from the North Atlantic and Arctic Oceans, including Davis Straits and Baffin's Bay: Philosophical Transactions of the Royal Society of London, 155, p. 325–441.

Pike J., Crosta, X., Maddison, E. J., Stickley, C. E., Denis, D., Barbara, L., and Rensenn, H., 2009, Observations on the relationship between the Antarctic coastal diatoms Thalassiosira Antarctica Comber and Porosira glacialis (Grunow) JØrgensen and sea ice concentrations during the Late Quaternary: Marine Micropaleontology, 73,1-2, p.14-25.

Pritchard, H. D., Ligtenberg, S. R. M., Fricker, H. A., Vaughan, D. G., van den Broeke, M. R., and Padman, L., 2012, Antarctic ice-sheet loss driven by basal melting of ice shelves: Nature London. 484, 7395, p. 502-505.

Pudsey, C. J., Barker, P. F., and Larter, R. D., 1994, Ice sheet retreat from the Antarctic Penisula Shelf: Continental Shelf Research. 14, p. 1647-1675.

Pudsey, C.J. and Evans, J., 2001, First survey of Antarctic sub-ice shelf sediments reveals mid-Holocene ice shelf retreat: Geology, 29, p. 787–90.

Pudsey, C.J., Murray, J.W., Appleby, P. and Evans, J., 2006, Ice shelf history from petrographic and foraminiferal evidence: Northeast AP: Quaternary Science Reviews, 25, p. 2357–79.

Rebesco, M., Camerlenghi, A., and Zanolla, C., 1998, Bathymetry and morphogenesis of the continental margin west of the AP: *Terra Antart*, 5, 4, p. 715-725.

Scambos, T., Hulbe, C., Fahnestock, M., 2003, Climate-induced ice shelf disintegration in the AP. In: Domack, E.W., Leventer, A., Burnett, A., Bindschadler, R., Convey, P., Kirby, M. (Eds.), AP Climate Variability: Historical and Palaeoenvironmental Perspectives. American Geophysical Union, Antarctic Research Series, 79, pp. 79-92. Washington, D.C.

Schmiedl, G., A. Mackensen., and Mueller, P.J., 1997, Recent foraminifera from the eastern South Atlantic Ocean: Dependence on food supply and water masses: Marine Micropaleontol., 32, p. 249-287.

Schroeder, C. J., D. B. Scott and F. S. Medioli, 1987, Can smaller benthic foraminifera be ignored in paleoenvironmental analyses?: J. Foram. Res., 17, p. 101-105.

Scott, D. B., Schafer, C. T., and Medioli, F. S., 1980, Eastern Canadian estuarine foraminifera: a framework for comparison: Journal of Foraminiferal Research, 10, p. 205–234.

Seguenza, G., 1862, Dei terreni Terziarii del distretto di Messina. Parte II — Descrizione dei foraminiferi monotalamici delle marne mioceniche del distrettodi Messina: T. Capra, Messina, 84.

Shackleton, N.J., 1987, Oxygen isotopes, ice volume and sea level: Quat. Sci. Rev., 6, p. 183-190.

Shevenell, A.E., Domack, E.W. and Kernan, G., 1996, Record of Holocene paleoclimate change along the AP: evidence from glacial marine sediments, Lallemand Fjord. In Banks, M.R. and Brown, M.J., editors, Climate succession and glacial record of the Southern Hemisphere: Proceedings of the Royal Society of Tasmania*,* 130, p. 55–64.

Shevenell, A.E. and Kennett, J.P., 2002, Antarctic Holocene climate change: a benthic foraminiferal stable isotope record from Palmer Deep: Palaeoceanography, 17, p. 1019.

Siegert, M.J., 2008, Antarctic subglacial topography and ice-sheet evolution: Earth Surface Processes and Landforms, 33, p. 646-660.

Sievers, H.A., and W.D. Nowlin, Jr., 1984, The stratification and water masses at Drake Passage: J. Geophys. Res., 89, p. 10,489-10,514.

Sjunneskog, C. and Taylor, F., 2002, Postglacial marine diatom record of the Palmer Deep, AP (ODP Leg 178, Site1098): Paleoceanography*,* 17.

Smith, R. C., Ainley, D., Baker, K., Domack, E., Emslie, S., Fraser, S., Kennett, Leventer, A., Mosley-Thompson, E., Stammerjohn, S., and Vernet, M., 1999, Marine ecosystem sensitivity to climate change: Bioscience, 49, 5, p. 393-404.

Stark, P., 1994, Climatic warming in the central AP area: Weather. 49, p. 215-220.

Stein, M., Heywood, R.B., 1994. Antarctic environment-physical oceanography: The AP and Southwest Atlantic region of the Southern Ocean, In: El-Sayed,S.Z.(Ed.), Southern Ocean Ecology. Cambridge University Press, Cambridge, p. 11—24.

Stuiver, M., Polach, H.A., 1977, Discussion: reporting of 14C data: Radiocarbon 19, 3, p. 355–63.

Summerhayes, C.P., Ainley, D., Barrett, P., Bindschadler, R., Clarke, A., Convey, P., Fahrbach, E., Gutt, J., Hodgson, D.A., Meredith, M.P., Murray, A.S., Pörtner, H.-O., di Prisco, G., Schiel, K., Speer, K., Turner, J., Verde, C., Willems, A., 2009, The Antarctic Environment in the Global System. In: Turner, J., Bindschadler, R., Convey, P., di Prisco, G., Fahrbach, E., Gutt, J., Hodgson, D.A., Mayewski, P.A., Summerhayes, C.P. (Eds.), Antarctic Climate Change and the Environment. Scientific Committee on Antarctic Research, Cambridge, pp. 1-32.

Szymcek P., Ishman S., Domack E., and Leventer A. 2007, Holocene oceanographic and climatic variability of the Vega Drift deduced through foraminiferal interpretation: 10th International Symposium on Antarctic Sciences.

Verbanaz, R. and Ishman, S.E. (in review) Paleoceanographic and paleoglacial reconstruction of Barilari Bay, western AP from the benthic foraminiferal record: Palaeogeography, Palaeoclimatology, Palaeoecology.

Wiesner H. 1931, Die Foraminiferen der deutschen Südpolar−Expedition 1901−1903: Deustche Südpolar−Expedition, Zoologie 20, p. 53–165.

Williamson, W. C., 1858, On the Recent Foraminifera of Great Britain: Ray Society, London, 107 p.

Willmott, V., Domack, E.W., Padman, L., and Canals, M., 2007, Glaciomarine sediment drifts from Gerlache Strait, AP: Glacial Sedimentary Processes and Products, p. 67-84.

Yoon, S.H. and Chough, S.K., 1993, Sedimentary characteristics of Late Pleistocene bottom current deposits, Barents Sea slope off northern Norway: Sed. Geol., 82, p. 33–45.

APPENDICES

APPENDIX A

Plate 1: Common Calcareous Foraminifera

1a: *Globocassidulina biora*

1b: *Globocassidulina subglabosa*

2: *Fursenkoina* spp.

3a,b: *Nonionella iridea*

4a,b: *Nonionella bradii*

5a,b,c: *Neogloboquadrina pachyderma*

6a,b: *Rosalina globularis*

7a,b: *Cibicides refulgens*

Plate 2: Common Agglutinated Foraminifera

1: *Miliammina arenacea*

2a,b: *Paratrochammina lepida*

3a,b: *Paratrochammina bartrami*

4: *Spiroplectammina biformis*

5a,b: *Portatrochammina antarctica*

6a,b: *Portatrochammina bipolaris*

7: *Rhumblerella* sp.

8: *Labrospira jeffreysii*

Plate 1: Common calcareous foraminifera.

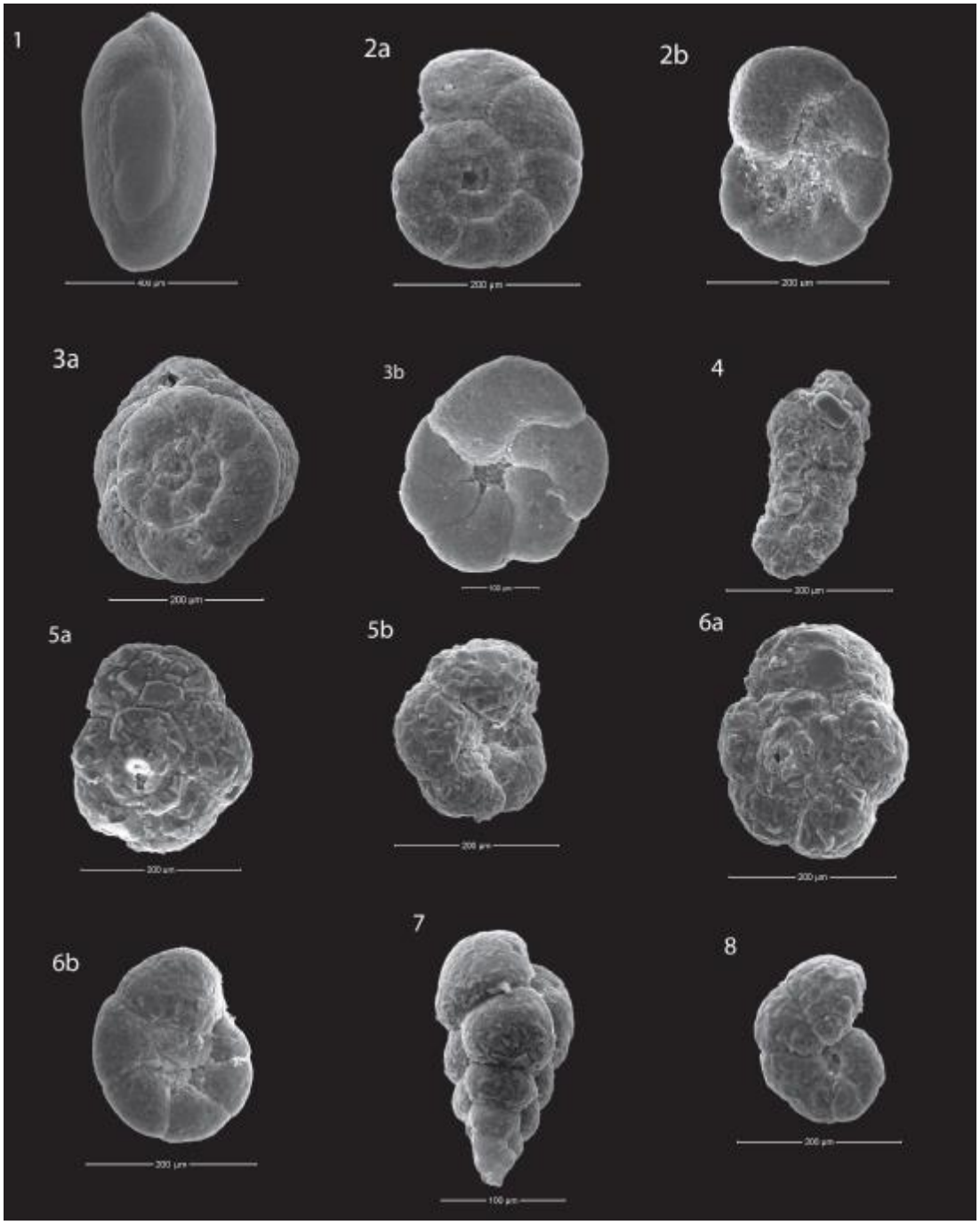

Plate 2: Common agglutinated foraminifera.

Depth (cm)	**4.5**	**10.5**	**20.5**	**30.5**	**40.5**	**50.5**	**60.5**	**70.5**	**80.5**	**90.5**	**100.5**	**110.5**	**120.5**	**130.5**	**140.5**	**150.5**
Milliamina arenacea	105	119	134	106	63	167	257	112	38	32	61	56	111	61	63	159
Milliamina lata	1	2	2	0	2	4	6	2	0	0	3	0	4	1	0	3
Haplophragmoides bradyi	6	6	1	0	0	0	0	0	1	1	0	1	1	0	0	0
Portatrochammina pseudotricamerata	3	1	2	4	0	2	1	2	2	2	7	0	3	1	1	1
Portatrochammina tricamerata	11	4	7	9	4	6	1	0	0	1	14	4	2	2	3	1
Portatrochammina bipolaris	8	6	7	3	0	3	7	3	2	9	2	4	4	0	4	2
Portatrochammina antarctica	10	14	20	16	4	29	17	17	14	13	23	33	44	28	14	12
Spiroplectammina biformis	11	12	8	3	1	3	0	20	18	11	116	54	30	39	63	136
Paratrochammina lepida	14	52	60	46	33	56	91	126	124	178	152	95	177	170	152	66
Atercotryma glomeratum	2	0	2	5	0	1	0	2	3	9	1	3	5	0	0	0
Labrospira jeffreysii	7	5	8	8	2	6	0	4	3	3	4	2	5	5	6	7
Textularia wiesneri	1	3	1	2	0	2	0	2	13	1	1	19	10	9	7	19
Rhambdammina sp.	2	8	3	1	0	0	3	5	3	6	2	5	3	7	4	5
Rhumblerella sp.	1	0	3	2	1	0	1	7	10	10	15	32	36	25	21	34
Paratrochammina bartmani	2	5	9	8	5	8	14	11	13	7	9	4	9	10	7	7
Laggenammina arenulata	0	1	0	0	0	0	0	0	0	0	0	0	0	0	0	0
Cystammina pauciloulata	0	0	0	0	0	0	0	0	0	0	0	0	0	0	0	0
Pseudobolivina antarctica	0	0	0	0	0	0	0	0	2	0	1	0	2	0	0	1

Depth (cm)	**160.5**	**170.5**	**180.5**	**190.5**	**200.5**	**210.5**	**220.5**	**230.5**	**240.5**	**250.5**	**260.5**	**270.5**	**280.5**	**290.5**	**300.5**
Milliamina arenacea	118	92	94	43	112	40	280	120	150	103	28	43	245	23	40
Milliamina lata	2	2	5	1	4	2	4	2	0	0	0	0	1	0	0
Haplophragmoides bradyi	0	0	0	0	0	0	0	0	0	0	0	0	0	0	0
Portatrochammina pseudotricamerata	2	2	6	0	2	2	0	2	0	2	0	0	0	0	0
Portatrochammina tricamerata	10	2	8	0	2	0	1	0	0	3	0	0	0	0	0
Portatrochammina bipolaris	11	6	7	4	3	3	1	8	3	7	3	9	2	0	2
Portatrochammina antarctica	15	11	28	12	19	9	11	20	20	29	10	16	15	8	17
Spiroplectammina biformis	0	11	38	12	68	9	50	13	124	31	18	16	47	20	24
Paratrochammina lepida	113	85	177	116	182	102	52	114	131	207	116	128	58	48	78
Atercotryma glomeratum	0	3	1	0	1	1	0	0	0	0	0	0	0	0	0
Labrospira jeffreysii	0	5	6	3	6	3	9	11	2	4	4	1	4	0	9
Textularia wiesneri	4	4	4	0	2	3	6	11	8	8	0	1	10	0	5
Rhambdammina sp.	4	3	8	0	5	3	2	0	2	0	2	4	1	0	0
Rhumblerella sp.	10	3	13	5	92	7	8	21	23	22	8	13	9	7	17
Paratrochammina bartmani	6	6	12	10	13	8	5	22	10	13	2	5	4	6	4
Laggenammina arenulata	0	0	0	0	0	0	0	0	0	0	0	0	0	0	0
Cystammina pauciloulata	0	0	0	0	0	0	0	0	0	0	0	0	0	0	0
Pseudobolivina antarctica	0	0	0	0	1	0	0	0	0	0	0	0	0	0	0

Appendix B: Agglutinated foraminifera counts (4.5 cm to 300.5 cm)

Depth (cm)	310.5	320.5	330.5	340.5	350.5	360.5	370.5	380.5	390.5	400.5	410.5	420.5	430.5	440.5	450.5
Milliamina arenacea	20	17	71	68	37	49	14	44	11	123	24	36	71	143	12
Milliamina lata	0	0	0	0	0	0	0	0	0	0	0	0	0	0	0
Haplophragmoides bradyi	0	0	0	0	0	0	0	0	0	0	0	0	0	0	0
Portatrochammina pseudotricamerata	0	0	0	1	0	0	0	0	0	0	0	0	0	0	0
Portatrochammina tricamerata	0	0	0	0	1	0	0	0	0	1	0	0	0	0	0
Portatrochammina bipolaris	0	1	3	3	0	3	1	3	2	0	0	0	0	0	0
Portatrochammina antarctica	8	4	16	15	18	7	1	3	0	3	0	7	2	4	4
Spiroplectammina biformis	20	7	43	36	36	33	5	0	0	2	0	0	0	3	1
Paratrochammina lepida	35	13	76	31	42	74	22	38	31	34	23	29	66	149	19
Atercotryma glomeratum	0	0	1	0	0	0	0	0	0	0	0	0	0	0	0
Labrospira jeffreysii	1	5	6	3	6	2	2	0	1	1	1	0	0	0	0
Textularia wiesneri	2	0	4	2	2	0	0	0	0	0	0	0	1	0	0
Rhambdammina sp.	0	0	0	0	0	0	0	0	0	0	0	0	0	0	0
Rhumblerella sp.	10	5	17	5	21	9	3	0	0	0	0	0	0	0	0
Paratrochammina bartmani	2	3	7	5	7	5	3	3	3	11	1	1	4	3	1
Laggenammina arenulata	0	0	0	0	0	0	0	0	0	0	0	0	0	0	0
Cystammina pauciloulata	0	0	0	0	0	0	0	0	0	0	0	0	0	0	0
Pseudobolivina antarctica	1	0	0	0	0	0	0	0	0	0	0	0	0	0	0

Depth (cm)	460.5	470.5	480.5	490.5	500.5	510.5	520.5	530.5	540.5	550.5	560.5	570.5	580.5	590.5	600.5
Milliamina arenacea	112	62	190	24	149	55	82	56	12	59	32	54	32	39	45
Milliamina lata	0	0	5	0	0	0	1	0	0	0	0	0	0	0	1
Haplophragmoides bradyi	0	0	0	0	0	0	0	0	0	0	0	0	0	0	0
Portatrochammina pseudotricamerata	0	1	0	0	0	0	1	1	0	0	0	0	0	0	0
Portatrochammina tricamerata	0	0	0	0	0	0	0	0	0	0	0	0	0	0	0
Portatrochammina bipolaris	0	0	1	0	0	2	3	4	0	0	0	0	0	0	0
Portatrochammina antarctica	9	9	4	6	7	10	21	22	3	11	6	3	2	5	6
Spiroplectammina biformis	0	2	14	1	16	2	26	35	7	2	31	13	3	1	2
Paratrochammina lepida	42	50	76	41	132	96	126	145	50	43	62	13	6	28	16
Atercotryma glomeratum	0	0	0	0	0	0	0	0	0	0	0	0	0	0	0
Labrospira jeffreysii	1	0	0	0	0	1	7	2	1	0	2	0	1	0	0
Textularia wiesneri	0	1	2	0	0	0	1	2	0	0	0	0	0	0	0
Rhambdammina sp.	0	0	0	0	0	0	0	0	0	0	0	0	0	0	0
Rhumblerella sp.	3	1	0	0	3	4	20	5	1	3	1	3	0	0	0
Paratrochammina bartmani	3	5	4	0	4	5	7	12	1	0	3	0	1	4	1
Laggenammina arenulata	0	0	0	0	0	0	0	0	0	0	0	0	0	0	0
Cystammina pauciloulata	0	0	0	0	0	0	0	0	1	0	1	0	0	1	1
Pseudobolivina antarctica	0	1	0	0	0	0	0	0	0	0	0	0	0	0	0

Appendix B: Agglutinated foraminifera counts (310.5 cm to 600.5 cm)

Depth (cm)	610.5	620.5	630.5	640.5	650.5	660.5	670.5	680.5	690.5	700.5	710.5	720.5	730.5	740.5	750.5
Milliamina arenacea	41	33	50	61	105	33	16	4	58	103	33	15	59	52	46
Milliamina lata	2	0	0	0	1	0	0	3	0	2	0	0	2	0	1
Haplophragmoides bradyi	0	0	0	0	0	0	0	0	0	0	0	0	0	0	0
Portatrochammina pseudotricamerata	0	0	0	0	0	0	0	0	0	0	0	0	0	0	0
Portatrochammina tricamerata	0	0	0	0	0	0	0	0	0	0	0	0	0	0	0
Portatrochammina bipolaris	0	0	0	0	1	0	0	0	0	0	0	0	0	0	1
Portatrochammina antarctica	6	4	10	5	8	2	4	5	0	0	1	2	1	1	0
Spiroplectammina biformis	1	11	5	5	14	3	16	3	1	6	5	2	1	3	0
Paratrochammina lepida	12	19	40	9	56	11	11	8	8	12	8	9	3	7	1
Atercotryma glomeratum	0	1	1	0	0	0	0	0	0	0	0	0	0	0	0
Labrospira jeffreysii	0	2	0	0	0	0	0	0	1	0	0	0	0	0	0
Textularia wiesneri	0	0	0	0	0	0	0	1	0	0	0	0	0	0	0
Rhambdammina sp.	0	0	0	0	0	0	0	0	0	0	0	0	0	0	0
Rhumblerella sp.	0	0	0	0	0	1	1	1	0	0	0	0	0	0	0
Paratrochammina bartmani	0	2	5	4	0	1	2	0	0	1	1	1	2	0	0
Laggenammina arenulata	0	0	0	0	0	0	0	0	0	0	0	0	0	0	0
Cystammina pauciloulata	0	0	0	0	0	0	0	0	0	0	0	0	0	0	0
Pseudobolivina antarctica	0	0	0	0	0	0	0	0	0	0	0	0	0	0	0

Depth (cm)	760.5	770.5	780.5	790.5	800.5	810.5	820.5	830.5	840.5	850.5	860.5	870.5	880.5	900.5	936.5
Milliamina arenacea	33	21	23	18	6	15	30	158	193	87	39	98	142	14	6
Milliamina lata	1	0	0	0	0	0	0	0	0	0	0	0	0	0	0
Haplophragmoides bradyi	0	0	0	0	0	0	0	0	0	0	0	0	0	0	0
Portatrochammina pseudotricamerata	0	0	0	0	0	0	0	0	0	0	0	0	0	0	0
Portatrochammina tricamerata	0	0	0	0	0	0	0	0	0	0	0	0	0	0	0
Portatrochammina bipolaris	0	0	0	0	0	0	0	0	0	0	0	0	0	0	0
Portatrochammina antarctica	0	0	0	0	0	0	0	0	0	0	0	0	0	0	0
Spiroplectammina biformis	0	0	0	0	0	0	0	0	0	0	0	0	0	0	0
Paratrochammina lepida	9	5	4	2	0	1	0	2	6	7	0	1	1	0	0
Atercotryma glomeratum	0	0	0	0	0	0	0	0	0	0	0	0	0	0	0
Labrospira jeffreysii	0	1	0	0	0	0	0	0	0	0	0	0	0	0	0
Textularia wiesneri	0	0	0	0	0	0	0	0	0	0	0	0	0	0	0
Rhambdammina sp.	0	0	0	0	0	0	0	0	0	0	0	0	0	0	0
Rhumblerella sp.	0	0	0	0	0	0	0	0	0	0	0	0	0	0	0
Paratrochammina bartmani	2	0	1	1	0	0	1	0	2	1	0	0	0	0	0
Laggenammina arenulata	0	0	0	0	0	0	0	0	0	0	0	0	0	0	0
Cystammina pauciloulata	0	0	0	0	0	0	0	0	0	0	0	0	0	0	0
Pseudobolivina antarctica	0	0	0	0	0	0	0	0	0	0	0	0	0	0	0

Appendix B: Agglutinated foraminifera counts (610.5 cm to 936.5 cm)

Depth (cm)	4.5	10.5	20.5	30.5	40.5	50.5	60.5	70.5	80.5	90.5	100.5	110.5	120.5	130.5	140.5	150.5
Fursenkoina spp.	0	0	0	0	0	0	0	0	0	0	0	0	0	0	0	0
Stainforthia davisi	0	0	0	0	0	0	0	0	0	0	0	0	0	0	0	0
Neogloboquadrina pachyderma	0	0	0	0	0	0	0	0	0	0	0	0	0	0	0	0
Astrononion echolsi	0	0	0	0	0	0	0	0	0	0	0	0	0	0	0	0
Cibicides refulgens	0	0	0	0	0	0	0	0	0	0	0	0	0	0	0	0
Globocassidulina spp.	0	0	0	0	0	0	0	0	0	0	0	0	0	0	0	0
A. earlandi	0	0	0	0	0	0	0	0	0	0	0	0	0	0	0	0
Rosalina globularis	0	0	0	0	0	0	0	0	0	0	0	0	0	0	0	0
Nonionella iridea	0	0	0	0	0	0	0	0	0	0	0	0	0	0	0	0
Nonionella bradii	0	0	0	0	0	0	0	0	0	0	0	0	0	0	0	0
F.crebra	0	0	0	0	0	0	0	0	0	0	0	0	0	0	0	0
Bulimina aculeata	0	0	0	0	0	0	0	0	1	0	0	0	0	0	0	0
H. gracillima	0	0	0	0	0	0	0	0	0	0	0	0	0	0	0	0
P. quinqueloba	0	0	0	0	0	0	0	0	0	0	0	0	0	0	0	0
Pseudoolina sp.	0	0	0	0	0	0	0	0	0	0	0	0	0	0	0	0
Cassidulinoides porrectus	0	0	0	0	0	0	0	0	0	0	0	0	0	0	0	0
H. cf. *sahulense*	0	0	0	0	0	0	0	0	0	0	0	0	0	0	0	0
Lagena sp.	0	0	0	0	0	0	0	0	0	0	0	0	0	0	0	0
Astrononion antarcticum	0	0	0	0	0	0	0	0	0	0	0	0	0	0	0	0
Cassidulinoides parvus	0	0	0	0	0	0	0	0	0	0	0	0	0	0	0	0
Oridorgalis sidebottomi	0	0	0	0	0	0	0	0	0	0	0	0	0	0	0	0

Depth (cm)	160.5	170.5	180.5	190.5	200.5	210.5	220.5	230.5	240.5	250.5	260.5	270.5	280.5	290.5	300.5
Fursenkoina spp.	0	0	0	0	0	21	0	0	0	0	0	0	0	305	87
Stainforthia davisi	0	0	0	0	0	1	0	0	0	0	0	0	0	4	3
Neogloboquadrina pachyderma	0	0	0	0	0	14	0	0	0	0	0	0	0	56	10
Astrononion echolsi	0	0	0	0	0	1	0	0	0	0	0	0	0	1	1
Cibicides refulgens	0	0	0	0	0	1	0	0	0	0	0	0	0	1	1
Globocassidulina spp.	0	0	0	0	0	4	0	0	0	0	0	2	0	7	16
A. earlandi	0	0	0	0	0	0	0	0	0	0	0	1	0	0	0
Rosalina globularis	0	0	0	0	0	0	0	0	0	0	0	0	0	3	3
Nonionella iridea	0	0	0	0	0	0	0	0	0	0	0	0	0	46	5
Nonionella bradii	0	0	0	0	0	0	0	0	0	0	0	0	0	14	0
F.crebra	0	0	0	0	0	0	0	0	0	0	0	0	0	1	0
Bulimina aculeata	0	0	0	0	0	0	0	0	0	0	0	0	0	10	0
H. gracillima	0	0	0	0	0	0	0	0	0	0	0	0	0	0	0
P. quinqueloba	0	0	0	0	0	0	0	0	0	0	0	0	0	0	0
Pseudoolina sp.	0	0	0	0	0	0	0	0	0	0	0	0	0	0	0
Cassidulinoides porrectus	0	0	0	0	0	0	0	0	0	0	0	0	0	0	0
H. cf. *sahulense*	0	0	0	0	0	0	0	0	0	0	0	0	0	0	0
Lagena sp.	0	0	0	0	0	0	0	0	0	0	0	0	0	0	0
Astrononion antarcticum	0	0	0	0	0	0	0	0	0	0	0	0	0	0	0
Cassidulinoides parvus	0	0	0	0	0	0	0	0	0	0	0	0	0	0	0
Oridorgalis sidebottomi	0	0	0	0	0	0	0	0	0	0	0	0	0	0	0

Appendix B: Calcareous foraminifera counts (4.5 cm to 300.5 cm)

Depth (cm)	310.5	320.5	330.5	340.5	350.5	360.5	370.5	380.5	390.5	400.5	410.5	420.5	430.5	440.5	450.5
Fursenkoina spp.	203	229	1	0	205	96	215	0	0	0	18	0	0	2	136
Stainforthia davisi	6	7	0	0	11	1	20	0	0	0	1	0	0	0	4
Neogloboquadrina pachyderma	67	21	0	0	23	19	11	0	0	0	0	0	0	0	50
Astrononion echolsi	0	0	0	0	0	0	0	0	0	0	0	0	0	0	1
Cibicides refulgens	1	1	0	0	0	1	0	0	0	0	0	0	0	0	0
Globocassidulina spp.	9	35	0	0	7	5	4	0	0	0	0	0	0	0	33
A. earlandi	0	0	0	0	0	3	1	0	0	0	0	0	0	0	3
Rosalina globularis	4	1	0	0	3	0	2	0	0	0	0	0	0	0	2
Nonionella iridea	38	20	0	0	15	3	65	0	0	0	0	0	0	0	106
Nonionella bradii	6	6	0	0	5	34	8	0	0	0	0	0	0	0	30
F.crebra	0	0	0	0	0	3	1	0	0	0	0	0	0	0	1
Bulimina aculeata	0	0	0	0	0	1	0	0	0	0	0	0	0	0	0
H. gracillima	1	0	0	0	0	0	0	0	0	0	0	0	0	0	0
P. quinqueloba	0	0	0	0	0	0	0	0	0	0	0	0	0	1	0
Pseudoolina sp.	0	0	0	0	0	0	0	0	0	0	0	0	0	0	1
Cassidulinoides porrectus	0	0	0	0	0	0	0	0	0	0	0	0	0	0	0
H. cf. *sahulense*	0	0	0	0	0	0	0	0	0	0	0	0	0	0	0
Lagena sp.	0	0	0	0	0	0	0	0	0	0	0	0	0	0	0
Astrononion antarcticum	0	0	0	0	0	0	0	0	0	0	0	0	0	0	0
Cassidulinoides parvus	0	0	0	0	0	0	0	0	0	0	0	0	0	0	0
Oridorgalis sidebottomi	0	0	0	0	0	0	0	0	0	0	0	0	0	0	0
Depth (cm)	**460.5**	**470.5**	**480.5**	**490.5**	**500.5**	**510.5**	**520.5**	**530.5**	**540.5**	**550.5**	**560.5**	**570.5**	**580.5**	**590.5**	**600.5**
Fursenkoina spp.	0	2	0	41	0	0	0	22	1	0	0	218	10	106	0
Stainforthia davisi	0	0	0	0	0	0	0	0	0	0	0	1	0	0	0
Neogloboquadrina pachyderma	0	4	1	16	0	9	6	27	6	0	0	27	20	34	8
Astrononion echolsi	0	0	0	0	0	0	0	1	2	0	0	1	0	0	0
Cibicides refulgens	0	0	0	1	0	6	1	9	1	0	0	0	2	5	1
Globocassidulina spp.	0	2	0	6	0	19	3	13	4	2	1	6	23	26	8
A. earlandi	0	1	0	0	0	1	0	2	0	0	0	1	1	2	0
Rosalina globularis	0	0	0	0	0	0	0	3	0	0	0	2	0	6	0
Nonionella iridea	0	0	0	0	0	0	0	0	0	0	0	26	0	5	0
Nonionella bradii	0	0	0	0	0	0	1	0	0	0	0	1	0	0	0
F.crebra	0	0	0	0	0	0	0	0	0	0	0	0	0	2	0
Bulimina aculeata	0	0	0	0	0	0	0	0	0	0	0	0	0	3	0
H. gracillima	0	0	0	0	0	0	0	0	0	0	0	0	0	0	0
P. quinqueloba	0	0	0	0	0	0	0	1	0	0	0	0	0	0	0
Pseudoolina sp.	0	0	0	0	0	0	0	0	0	0	0	0	0	0	0
Cassidulinoides porrectus	0	0	0	0	0	0	0	0	1	0	0	0	0	0	0
H. cf. *sahulense*	0	0	0	0	0	0	0	0	0	0	0	0	0	0	0
Lagena sp.	0	0	0	0	0	0	0	0	0	0	0	0	0	0	0
Astrononion antarcticum	0	0	0	0	0	0	0	0	0	0	0	0	0	0	0
Cassidulinoides parvus	0	0	0	0	0	0	0	0	0	0	0	0	0	0	0
Oridorgalis sidebottomi	0	0	0	0	0	0	0	0	0	0	0	0	0	0	0

Appendix B: Calcareous foraminifera counts (310.5 cm to 600.5 cm)

Depth (cm)	610.5	620.5	630.5	640.5	650.5	660.5	670.5	680.5	690.5	700.5	710.5	720.5	730.5	740.5	750.5
Fursenkoina spp.	16	127	3	0	0	4	0	14	1	1	211	151	112	8	0
Stainforthia davisi	0	0	0	0	0	0	0	0	0	0	8	4	3	0	0
Neogloboquadrina pachyderma	7	32	6	0	0	4	0	25	8	7	48	75	17	8	0
Astrononion echolsi	0	2	0	0	0	0	0	0	0	0	1	0	1	0	0
Cibicides refulgens	1	11	1	0	0	3	0	2	3	0	0	0	0	0	0
Globocassidulina spp.	6	43	35	0	0	5	0	19	1	4	17	21	103	23	0
A. earlandi	1	0	0	0	0	0	0	3	1	0	0	1	4	0	0
Rosalina globularis	0	14	0	0	0	1	0	0	1	0	2	2	5	0	0
Nonionella iridea	0	17	0	0	0	0	0	0	0	0	26	110	14	0	0
Nonionella bradii	0	11	0	0	0	0	0	0	0	0	15	44	5	1	0
F.crebra	1	1	0	0	0	0	0	0	0	0	1	0	0	0	0
Bulimina aculeata	0	0	0	0	0	1	0	0	2	0	0	0	0	0	0
H. gracillima	0	0	0	0	0	0	0	0	0	0	2	0	0	0	0
P. quinqueloba	0	0	0	0	0	0	0	0	0	0	0	0	0	0	0
Pseudoolina sp.	0	0	0	0	0	0	0	0	0	0	0	0	0	0	0
Cassidulinoides porrectus	0	0	0	0	0	1	0	1	1	0	0	1	0	0	0
H. cf. *sahulense*	0	1	0	0	0	0	0	0	0	0	0	1	0	0	0
Lagena sp.	0	1	0	0	0	0	0	0	0	0	0	0	0	1	0
Astrononion antarcticum	0	0	0	0	0	0	0	0	0	0	0	0	0	0	0
Cassidulinoides parvus	0	0	0	0	0	0	0	0	0	0	0	0	0	0	0
Oridorgalis sidebottomi	0	0	0	0	0	0	0	0	0	0	0	0	0	0	0
Depth (cm)	**760.5**	**770.5**	**780.5**	**790.5**	**800.5**	**810.5**	**820.5**	**830.5**	**840.5**	**850.5**	**860.5**	**870.5**	**880.5**	**900.5**	**936.5**
Fursenkoina spp.	0	0	0	165	0	0	0	0	30	27	39	0	11	186	58
Stainforthia davisi	0	0	0	3	0	0	0	0	0	0	0	0	0	11	3
Neogloboquadrina pachyderma	0	0	0	6	0	0	0	0	1	18	0	0	2	1	2
Astrononion echolsi	0	0	0	1	0	0	0	0	0	3	1	1	1	0	0
Cibicides refulgens	0	0	0	0	0	0	0	0	5	1	1	0	1	0	0
Globocassidulina spp.	0	0	0	113	0	0	0	0	1	9	1	0	32	142	254
A. earlandi	0	0	0	3	0	0	0	0	0	4	2	0	0	0	0
Rosalina globularis	0	0	0	1	0	0	0	0	0	1	0	0	1	0	0
Nonionella iridea	0	0	0	11	0	0	0	0	0	143	11	0	0	4	2
Nonionella bradii	0	0	0	11	0	0	0	0	2	11	5	0	0	0	0
F.crebra	0	0	0	0	0	0	0	0	0	0	0	0	0	0	0
Bulimina aculeata	0	0	0	0	0	0	0	0	0	0	0	0	0	0	0
H. gracillima	0	0	0	0	0	0	0	0	0	0	0	0	0	0	0
P. quinqueloba	0	0	0	0	0	0	0	0	0	0	0	0	0	0	0
Pseudoolina sp.	0	0	0	0	0	0	0	0	0	0	0	0	0	0	0
Cassidulinoides porrectus	0	0	0	0	0	0	0	0	0	0	0	0	0	0	0
H. cf. *sahulense*	0	0	0	0	0	0	0	0	0	1	0	0	0	0	0
Lagena sp.	0	0	0	0	0	0	0	0	0	0	0	0	0	0	0
Astrononion antarcticum	0	0	0	1	0	0	0	0	0	0	0	0	0	0	0
Cassidulinoides parvus	0	0	0	0	0	0	0	0	0	1	0	0	0	0	0
Oridorgalis sidebottomi	0	0	0	0	0	0	0	0	0	0	1	0	0	0	0

Appendix B: Calcareous foraminifera counts (610.5 cm to 936.5 cm)

Appendix C: Foraminiferal Systematics

Angulogerina earlandi – Parr, (1950). Igarashi et al., (2001, pl. 11, fig. 7).

Astrononion antarcticum – Parr, (1950). Igarashi *et al.,* (2001, pl. 12, fig. 10).

Astrononion echolsi – Kennett, (1967). Majewski, (2005, fig. 25.6–7).

Adercotryma glomerata – Brady, (1878). Majewski, (2005, fig. 14.1).

Bulimina aculeata - d'Orbigny, (1826). Igarashi et al., (2001, pl. 11, fig. 4).

Cassidulinoides parvus – Earland, (1934). Igarishi et al., (2001, pl. 10, fig 11).

Cassidulinoides porrectus - Heron−Allen and Earland, (1932). Majewski, (2005, fig. 23.3).

Cibicides refulgens - de Montfort, (1808). Majewski, (2005, fig. 25.1).

Cystammina pauciloculata = *Trochammina pauciloculata* – Brady, (1879). Igarashi et al., (2001, pl. 3, fig. 1).

Fissurina crebra - Matthes, (1939). Majewski, (2005, fig. 21.8).

Fursenkoina spp. – Includes *Fursenkoina fusiformis* - Williamson, (1858). Majewski, (2005, fig. 23.9–12). Also includes *Fursenkoina vestfoldensis* – Crespin, 1960. Igarashi (2001, pl. 11, fig. 6).

Globocassidulina spp. - Includes *Globocassidulina biora* - Crespin, (1960), Majewski, (2005, fig. 23.4–8). Also includes *Globocassidulina subglabosa*.

Hyalinonetrion sahulense – Patterson and Richardson, (1988). Igarashi et al., (2001, pl. 6, fig. 14)

Hyalinonetrion gracillima - Seguenza, (1862). Majewski, (2005, fig. 20.7).

Labrospira jeffreysii - Williamson, (1858). Majewski, (2005, fig. 13.14).

Lagena sp. - Includes *Lagena squamososulcata* - Heron−Allen and Earland, (1922). Majewski, (2005, fig. 20.11). Also includes *Lagena subacuticosta* - Parr, (1950). Majewski, (2005, fig. 20.8).

Lagenammina arenulata - Skinner, (1961). Majewski, (2005, figs 9.8–9, 9.12).

Miliammina arenacea - Chapman, (1916). Majewski, (2005, fig. 12.6–7).

Miliammina lata - Heron−Allen *and* Earland, (1930). Majewski, (2005, fig. 12.8).

Neogloboqudrina pachyderma = *Aristerospira pachyderma* – Ehrenberg, (1861). Igarashi et al., (2001, pl. 10, fig. 8,9).

Nonionella bradii - Chapman, (1916). Majewski, (2005, fig. 25.4–5).

Nonionella iridea - Herron−Allen and Earland, (1932). Majewski, (2005, fig. 25.2–3).

Oridorsalis sdebottomi = *Eponides sidebottomi* - Earland, (1934). Igarashi et al., (2001, pl. 12, fig, 12).

Pullenia quinqueloba = *Nonionina quinqueloba* – Reuss, (1851). Igarishi et al., (2001, pl. 12, fig. 9).

Paratrochammina bartrami - Hurdle and Burdett, (1967). Majewski, (2005, fig. 14.7–8).

Paratrochammina lepida - Brönnimann and Whittaker, (1988). Majewski, (2005, fig. 14.9–10).

Portatrochammina bipolaris – (Brönnimann and Whittaker, 1980). Majewski (2005, fig. 15.7–8).

Paratrochammina pseudotricamerata = *Trochammina pseudotricamerata* – Earland, (1934). Igarashi et al., (2001, pl. 4, fig. 4).

Paratrochammina tricamerata = *Trochammina tricamerata* – Earland, (1934). Igarashi et al., (2001, pl. 4, fig. 2).

Pseudobolivina antarctica – Wiesner, (1931). Igarashi et al., (2001, pl. 3, fig. 12).

Rhabdammina sp. – Majewski, (2005, fig. 9.3–5).

Rhumblerella sp. – Majewski, (2005, fig. 14.6).

Rosalina globularis - d'Orbigny, (1826). Majewski, (2005, fig. 24.1–4).

Spiroplectammina biformis - Parker and Jones, (1865). Majewski, (2005, fig. 14.3–5).

Stainforthia davisi = Virgulina davisi – Chapman and Parr, (1937). Igarashi, (2001, pl. 11, fig. 3).

Textularia wiesneri – Earland, (1933). Igarashi et al., (2001, pl. 6, fig. 3).

VITA

Graduate School
Southern Illinois University

Daniel J. Groves

djgrove@siu.edu

Illinois State University, Normal, IL
Bachelor of Science, Geology, May 2013

Special Honors and Awards:

Porter-Jobling Fellowship - (2014), Department of Geology, Southern Illinois University, Carbondale, IL

Thesis Title:

HOLOCENE FORAMINIFERAL ASSEMBLAGE AND STABLE ISOTOPE ANALYSIS FOR THE GERLACHE STRAIT, AP.

Major Professor: Scott Ishman